

ABSTRACT

Title of Thesis: **THREE-DIMENSIONAL
MOTION COORDINATION
IN A TIME-VARYING FLOWFIELD**

Sonia Hernandez-Doran, Master of Science, 2009

Thesis Directed By: **Dr. Derek A. Paley
Department of Aerospace Engineering**

Decentralized algorithms that stabilize three-dimensional formations of unmanned vehicles in a time-varying flowfield have applications in environmental monitoring in the atmosphere and ocean. This thesis provides Lyapunov-based algorithms to control a system of self-propelled particles traveling in three dimensions at a constant speed relative to a spatiotemporal flowfield. A particle's inertial velocity is the sum of its velocity relative to the flowfield plus the velocity of the flowfield. Multiple particles can be steered to form parallel, helical, and circular formations. A special case of the three-dimensional model is also studied, in which the particles travel on the surface of a sphere. In this case, we provide Lyapunov-based algorithms that stabilize circular formations in a time-varying flowfield on a rotating sphere. Because we are interested in using unmanned-vehicle formations for environmental monitoring, we simulate our results using numerical simulations of time-varying flowfields that resemble tornadoes and hurricanes.

Three-Dimensional Motion Coordination in a Time-Varying Flowfield

by

Sonia Hernandez-Doran

Thesis submitted to the Faculty of the Graduate School of the
University of Maryland, College Park in partial fulfillment
of the requirements for the degree of
Master of Science
2009

Advisory Committee:
Dr. Derek A. Paley
Dr. J. Sean Humbert
Dr. Amr Baz

© Copyright by
Sonia Hernandez-Doran
2009

Acknowledgments

The last two years at Maryland have been a great experience. I have grown both in knowledge and as a person during my time here. One of the most important accomplishments (besides learning LaTeX!) is that I have confirmed my wish to obtain a Ph.D. and become a professor. This couldn't have been possible without the help of so many incredible people.

Firstly, I'd like to dedicate this work to my advisor, Derek Paley. It saddens me to be leaving him because I know it will be very difficult to find someone who dedicates so much time and energy to his students. I couldn't have asked for a better advisor. He has been incredibly helpful and understandable, and his knowledge amazes me more and more every day. I am thankful for his patience and for all the time he has put into helping me shape this thesis. Without him, this work could have never been possible. Besides my thesis research, I also want to thank Derek for helping me become a better scientific writer with the many, many revisions we went through with our conference and journal papers. I admire him and aspire to be like him when I am a professor.

This thesis couldn't have been possible without the great friends I have made in the last few years. I would like to thank my incredible friend Rodrigo for his time and guidance trying to make me a better mathematician. Also, thanks to my roommates Scott, Kan, and Evan for their help and support. Living with them was a great experience that I will cherish forever. My labmates Sachit and Cammy have been exceptionally helpful. I am thankful to Darren for his help and encouragement,

and glad that our research has focused on similar topics in the last couple of years. I still hope to write a paper together in the future.

I am so thankful to have such wonderful parents. They have always been nothing but supportive of every decision I've made. I especially owe my gratitude to my dad for staying up late so many nights to help me. I admire how he works through problems, even if they're not in his area of expertise, and manages to help me solve them. He is someone that I look up to in my academic career. Thanks also goes to my sister Marlit because she always knows how to make me laugh and smile.

Last, but not least, I would like to thank Ryan for his support and patience the last few years. You are amazing and I hope we get to experience graduate school together some day.

Table of Contents

List of Figures	vi
1 Introduction	1
1.1 Previous Work	2
1.2 Contributions of the Thesis	4
1.3 Outline of the Thesis	6
2 Mathematical Preliminaries	8
2.1 Trajectory of a Particle	8
2.1.1 Moving Frames	8
2.1.2 Rotational Motion in \mathbb{R}^3 : $SO(3)$	9
2.1.3 Rigid Motion in \mathbb{R}^3 : $SE(3)$	11
2.1.4 Screw Theory	12
2.2 Nonlinear Control Theory	14
2.2.1 Stability of Autonomous Systems	15
2.2.2 Stability of Non-autonomous Systems	19
2.3 Graph Theory	20
2.3.1 Directed vs. Undirected Graphs	20
2.3.2 Laplacian Matrix	20
3 Particle Dynamics in a Time-Varying Flowfield	23
3.1 Particle Motion in Three Dimensions	23
3.1.1 Flow-Free Particle Dynamics	23
3.1.2 Particle Dynamics in a Time-Varying Flowfield	26
3.2 Particle Motion on a Rotating Sphere	30
3.2.1 Flow-Free Particle Dynamics	31
3.2.2 Particle Dynamics on a Rotating Sphere	32
3.2.3 Particle Dynamics in a Time-Varying Flowfield	36
4 Design of Decentralized Motion Coordination Algorithms	40
4.1 Stabilization of Parallel Formations in a Three-Dimensional Flowfield	40
4.1.1 Parallel Formation with Arbitrary Direction	41
4.1.2 Parallel Formation in a Prescribed Direction	43
4.2 Stabilization of Helical Formations in a Three-Dimensional Flowfield	45
4.2.1 Helical Formation with Arbitrary Pitch	46
4.2.2 Helical Formation with a Prescribed Pitch and Center	49
4.3 Stabilization of Circular Formations on a Rotating Sphere with Flow	53
4.3.1 Circular Formation on a Flow-Free Rotating Sphere	54
4.3.2 Circular Formation with Arbitrary Center	56
4.3.3 Circular Formation with a Prescribed Center	59

5	Conclusion	62
A	Transformation Between Relative and Inertial Path Frames	64
B	Proof of Theorem 4	67
C	Derivation of the Coriolis Acceleration	69
D	The 2-Vortex Problem	72
E	Proof of equation (4.3)	74
	Bibliography	76

List of Figures

1.1	School of fish traveling in a circular formation.	2
2.1	Trajectory of particle k in three dimensions.	10
2.2	Screw motion	13
2.3	Example of the stability of an autonomous system.	16
2.4	Example of (a) an undirected and (b) a directed graph.	21
2.5	Example of undirected communication topology with 5 agents	22
3.1	Schematic of vectors used in the three-dimensional motion models. . .	24
3.2	Schematic of <i>relative equilibria</i> of the flow-free three-dimensional model.	25
3.3	Reference frames used to derive particle dynamics on the sphere. . . .	33
3.4	Circular formation on a sphere	38
4.1	Stabilization of particle model (3.3) to parallel motion in an arbitrary direction in a time-varying flowfield using control (4.2)	44
4.2	Stabilization of particle model (3.3) to parallel motion with prescribed direction in a time-varying flowfield using control (4.5).	46
4.3	Stabilization of particle model (3.3) to helical motion in a time- varying flowfield with arbitrary pitch and center.	49
4.4	Stabilization particle model (3.3) to helical motion with zero pitch, which is a circular formation, using control (4.10).	52
4.5	Stabilization of particle model (3.3) to helical motion with prescribed pitch and center in a time-varying flowfield using control (4.13). . . .	54
4.6	Stabilization of model (3.14) to circular motion on a rotating sphere.	56
4.7	Stabilization of particle model (3.18) to circular motion in a time- varying flowfield generated by two point vortices.	60
D.1	Two point vortices generate a time-varying flow as they travel on the surface of a sphere.	73

Chapter 1

Introduction

Nature gives us many instances of animal species grouping together to move in a specific coordinated motion. The way a flock of birds or a swarm of insects collect and move together is a natural phenomenon to behold. Schools of fish turn instinctively based on the local interactions between individual fish, and their movement seems to travel through the entire school immediately, sometimes shaping the group into an incredible circular formation (see Figure 1) [22].

Engineers and scientists have been inspired to portray the collective motion behavior of biological species in collaborating systems of autonomous vehicles. *Cooperative control*, the study that generates collective motion using feedback control laws, has been used in many real-world applications in air [2], sea [19], and space [29]. Examples include Aerosonde unmanned aerial vehicles that fly into hurricanes to obtain flow data [10] and autonomous underwater gliders that provide a robust platform for synoptic data collection of spatiotemporal processes in the ocean [3].

An interesting trait of collective motion control is the decentralized manner by which unmanned vehicles (or agents) group together. This means that there is no common leader (as happens in centralized control systems). Even though biological species seem to collect and move almost effortlessly, for autonomous vehicles this is



Figure 1.1: School of fish traveling in a circular formation.

a major challenge. A group of agents collect into a formation through the process of *consensus*. Each agent may have limited communication and, therefore, may only know the location and/or orientation of some of the other agents. Moreover, knowledge of the desired formation may not be available to all the agents. The agents reach a desired formation by transmitting information repeatedly to other agents until *consensus* is achieved.

1.1 Previous Work

Cooperative control is a topic that has become very popular in the last ten years. The blossoming of this concept came with an article in the *Physical Review Letters* by Vicsek *et al.*, in which agents (modeled as particles) travel in a simple, planar model at the same speed but with a different direction of motion [35]. The agents change their heading by using the average direction of motion of their neighbors. Simulations show that, even though there is no leader in the group, the agents converge to the same heading [35]. This paper garnered great interest a few

years later in the controls community when Jadbabaie *et al.* published an article with a theoretical explanation for this observed behavior [11]. Since then, the topic of collective motion has expanded tremendously in several fields of study. Algorithms have been designed to model biological grouping behavior (such as flocking of birds or swarming of fish) and to model formation of unmanned vehicles (such as underwater gliders or aerial vehicles).

Graph theory was introduced in cooperative control in [4] and [18]. It provides a method to describe the interconnection between particles by means of a Laplacian matrix (see Section 2.3) and has been found to be of great use in deriving the necessary control laws to stabilize a system of agents. Graph theory can be used with particles that interact either with a fixed or a time-varying interaction network [23].

Most recent work on collective motion has focused on a *planar* model of self-propelled particles [12, 13, 17, 16, 25, 34]. This model consists of N identical self-propelled particles moving in a plane at unit speed. A steering control changes the heading of each particle until the system reaches the desired formation. In this system there are two types of steady-state formations in which the relative position and relative orientation of each particle remain fixed: parallel and circular motions [13]. Decentralized control algorithms that stabilize parallel and circular formations with all-to-all communication are given in [33] and, with limited communication, in [34]. Both these papers also address the issue of regulating spacing between particles. Motivated by real-world applications in which autonomous vehicles travel in the presence of a flow, a planar framework is presented in [26] which incorporates a time-invariant flowfield. This work is then extended to time-varying

flowfields in [28].

A planar model is sufficient for stabilizing collective motion in a small-scale operating domain. However, motivated by unmanned vehicles that operate in large planetary-scale sensing networks—such as underwater gliders and long-endurance aircraft—we are interested in looking at three-dimensional models. Most of the work done in *non-planar* collective motion has focused on flow-free models [5, 14, 30, 31]. Justh and Krishnaprasad present a model in which N self-propelled particles travel in three dimensions and a steering control changes the direction of motion of each particle [14]. Steady-state formations of this model are parallel, circular, and helical motions [14]. In [30], Scardovi *et al.* design decentralized control laws to stabilize these three types of motions in the presence of all-to-all communication. For constant altitude/depth surveys on scales where the curvature and/or rotation of the Earth are relevant, spherical models are relevant. Paley introduced a model in which N self-propelled particles constrained to travel on the surface of a sphere use a decentralized control law to achieve a circular formation [24].

1.2 Contributions of the Thesis

In this thesis we build upon the flow-free three-dimensional [30] and spherical [24] models by introducing a time-varying flowfield to both models. The three-dimensional analysis in this paper extends [31] and [30], which describe decentralized strategies to steer a three-dimensional system of self-propelled particles in a flow-free environment. To include a time-varying flowfield, we adapt the development of a

planar framework for collective motion in a time-varying flow [26]. We introduced a spatially variable, time-invariant flowfield to the three-dimensional model in [9]. We relax the all-to-all communication requirement in [9] to accommodate any connected and time-invariant communication topology. This can also be extended to directed, time-varying topologies [34].

The spherical analysis in this paper extends [24], which introduced a flow-free spherical model. Additional work appears in [8], in which we introduced rotation and a time-invariant flow to the spherical model. We study motion coordination in a time-varying flowfield on a rotating sphere because we are interested in creating a model to address applications where the rotation and curvature of the Earth are important.

For both the three-dimensional and spherical models we design Lyapunov-based decentralized control laws that stabilize particle formations. In the three-dimensional model we stabilize parallel and helical formations and, in the spherical model, we stabilize circular formations. A parallel formation is a steady motion in which all of the particles travel in straight, parallel lines with arbitrary separation. In a helical formation, all of the particles converge to circular helices with the same axis of rotation, radius of rotation, and pitch (the ratio of translational to rotational motion); the along-axis separation is arbitrary. A three-dimensional circular formation is a helical formation with zero pitch. These formations are relative equilibria of the flow-free three-dimensional particle model [14]. Decentralized controls to stabilize relative equilibria in the flow-free model are provided in [31]. On the sphere, a circular formation is a steady motion in which all of the particles

travel around a fixed circle on the sphere, with radius smaller than the radius of the sphere. Decentralized controls to stabilize circular formations on the sphere in the flow-free model are provided in [24].

The theoretical results are validated and extended by numerical simulations. In our simulations we choose circulating, time-varying flows that model naturally occurring phenomena such as hurricanes, tornadoes, and ocean currents. We are interested in these types of flows because formations of unmanned vehicles can be used for environmental monitoring. For example, in the three-dimensional model we illustrate the stabilization of a helical formation in a hurricane-inspired flowfield. Helical formations have the potential application of autonomous data collection inside a hurricane. In the rotating spherical model, we simulate the time-varying flowfield generated by two point vortices.

1.3 Outline of the Thesis

The thesis is organized as follows. In Chapter 2 we introduce the mathematical background necessary to follow the work that composes the thesis. In Chapter 3 we model a system of self-propelled particles in a time-varying flowfield that travel in three dimensions (Section 3.1) and on the surface of a rotating sphere (Section 3.2). Chapter 4 deals with deriving control laws to stabilize particle formations for both the three-dimensional and spherical models. In Section 4.1 we provide control laws for the three-dimensional model to stabilize parallel formations in either an arbitrary or a prescribed direction. In Section 4.2, we provide control laws for the three-

dimensional model to stabilize helical formations with arbitrary center and arbitrary or prescribed pitch or prescribed center and prescribed pitch. In Section 4.3 we provide control laws for the spherical model to stabilize circular formations with arbitrary or prescribed center. Chapter 5 summarizes the results and discusses future work.

Chapter 2

Mathematical Preliminaries

This chapter introduces the mathematical background necessary to understand the work and contributions that compose the thesis. In Section 2.1 we introduce the concepts of $SO(3)$ and $SE(3)$ that are used to represent the position and orientation of each agent in the systems we are studying. In Section 2.2 we describe pertinent concepts in the field of nonlinear control theory. In Section 2.3 we show that we can represent how each agent communicates with each other by means of a graph.

2.1 Trajectory of a Particle

In this thesis, we model nonlinear systems that consist of N agents (modeled as particles). In Section 2.1.1 we introduce the frame used to represent the three-dimensional trajectory that the particles trace. We show how to represent the velocity orientation of each particle in Section 2.1.2 and the position of each particle in Section 2.1.3. In Section 2.1.4 we show how screw motion and the concept of *twist* are used to represent the collective motion of a set of particles.

2.1.1 Moving Frames

A particle that moves in three dimensions traces out a trajectory $\gamma : [0, \infty) \rightarrow \mathbb{R}^3$ [14]. If the speed of the particle is unit, the curve γ needs to be at least twice

continuously differentiable and $|(d/dt)\boldsymbol{\gamma}| = 1 \forall t$, where t is time [14]. The direction of motion of the particle is the unit tangent vector to the trajectory. There is a gyroscopic force vector in the plane perpendicular to the tangent vector that steers each particle. We represent the equations of motion of a particle that traces out a curve $\boldsymbol{\gamma}$ using a natural Frenet frame [1, 14]

$$\begin{aligned}
\dot{\mathbf{r}}_k &= \mathbf{x}_k \\
\dot{\mathbf{x}}_k &= q_k \mathbf{y}_k + h_k \mathbf{z}_k \\
\dot{\mathbf{y}}_k &= -q_k \mathbf{x}_k + w_k \mathbf{z}_k \\
\dot{\mathbf{z}}_k &= -h_k \mathbf{x}_k - w_k \mathbf{y}_k,
\end{aligned} \tag{2.1}$$

where the position of particle k is \mathbf{r}_k and its velocity is $\dot{\mathbf{r}}_k$. The gyroscopic force $\mathbf{u}_k = [w_k \ -h_k \ q_k]^T \in \mathbb{R}^3$ steers the particle by rotating its velocity about the unit vectors of a path frame, $\mathcal{C}_k = (k, \mathbf{x}_k, \mathbf{y}_k, \mathbf{z}_k)$, which is fixed to particle k such that the unit vector \mathbf{x}_k points in the direction of the velocity of particle k (see Figure 2.1).

2.1.2 Rotational Motion in \mathbb{R}^3 : $SO(3)$

Consider a system of N particles, where the velocity of particle $k \in \{1, \dots, N\}$ has a specific orientation with respect to an inertial frame. The orientation of $\dot{\mathbf{r}}_k$ is given by a right-handed reference frame, with axes $\mathbf{x}_k, \mathbf{y}_k, \mathbf{z}_k \in \mathbb{R}^{3 \times 1}$ (see Figure 2.1). The 3×3 orthogonal matrix that defines the orientation of $\dot{\mathbf{r}}_k$ is $R_k = [\mathbf{x}_k \ \mathbf{y}_k \ \mathbf{z}_k]$. The *special orthogonal* group $SO(3)$ is the space of orthogonal matrices that represents the velocity orientation of particle k in $\mathbb{R}^{3 \times 3}$ and is defined

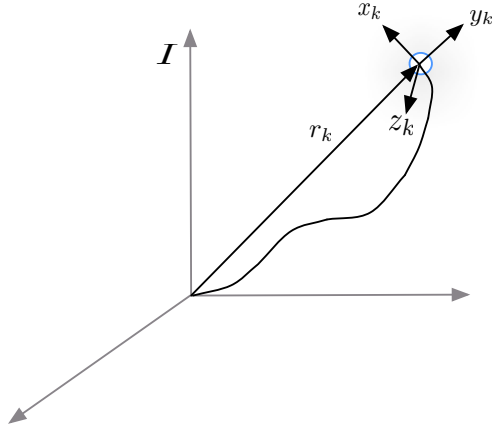


Figure 2.1: Trajectory of particle k in three dimensions, where the position of k is \mathbf{r}_k and the velocity orientation of k is given by a path frame $\mathcal{C}_k = (k, \mathbf{x}_k, \mathbf{y}_k, \mathbf{z}_k)$.

as [20]

$$SO(3) = \{R_k \in \mathbb{R}^{3 \times 3} : R_k R_k^T = I, \det(R_k) = 1\}, \quad (2.2)$$

where I is the 3×3 identity matrix.

Suppose we change the orientation of particle k by rotating it about an axis

$\boldsymbol{\omega} = [\omega_1 \ \omega_2 \ \omega_3]^T$. The time derivative of \mathbf{x}_k is

$$\dot{\mathbf{x}}_k = \boldsymbol{\omega} \times \mathbf{x}_k = \begin{vmatrix} \mathbf{x}_k & \mathbf{y}_k & \mathbf{z}_k \\ \omega_1 & \omega_2 & \omega_3 \\ 1 & 0 & 0 \end{vmatrix} = \omega_3 \mathbf{y}_k - \omega_2 \mathbf{z}_k.$$

Defining the skew-symmetric matrix

$$\hat{\boldsymbol{\omega}} = \begin{bmatrix} 0 & -\omega_3 & \omega_2 \\ \omega_3 & 0 & -\omega_1 \\ -\omega_2 & \omega_1 & 0 \end{bmatrix},$$

the rates of change of \mathbf{x}_k , \mathbf{y}_k , and \mathbf{z}_k are written in a compact form by [20]

$$\dot{R}_k = [\dot{\mathbf{x}}_k \ \dot{\mathbf{y}}_k \ \dot{\mathbf{z}}_k] = R_k \hat{\boldsymbol{\omega}}$$

The vector space of all 3×3 skew-symmetric matrices is denoted [20]

$$\mathfrak{so}(3) = \{\hat{\boldsymbol{\omega}} \in \mathbb{R}^{3 \times 3} : \hat{\boldsymbol{\omega}}^T = -\hat{\boldsymbol{\omega}}\}. \quad (2.3)$$

2.1.3 Rigid Motion in \mathbb{R}^3 : $SE(3)$

Consider a system of N particles, where each particle $k \in \{1, \dots, N\}$ has a specific position with respect to an inertial frame. We describe the position vector of k by $\mathbf{r}_k \in \mathbb{R}^3$ and the orientation of its velocity by $R_k \in SO(3)$ (see Figure 2.1). The pair (\mathbf{r}_k, R_k) is in the product space of \mathbb{R}^3 with $SO(3)$ and is defined as the *special Euclidian* group [20]

$$SE(3) = \{(\mathbf{r}_k, R_k) : \mathbf{r}_k \in \mathbb{R}^3, R_k \in SO(3)\} = \mathbb{R}^3 \times SO(3). \quad (2.4)$$

Following [20], suppose we change the position of particle k by translating it by an amount $\mathbf{q} \in \mathbb{R}^3$ and change the orientation of $\dot{\mathbf{r}}_k$ by rotating it about the axis $\boldsymbol{\omega} \in \mathbb{R}^3$. The time derivative of \mathbf{r}_k is

$$\dot{\mathbf{r}}_k = \boldsymbol{\omega} \times (\mathbf{r}_k - \mathbf{q}). \quad (2.5)$$

Defining the 4×4 matrix

$$\hat{\boldsymbol{\xi}} = \begin{bmatrix} \hat{\boldsymbol{\omega}} & \mathbf{v} \\ \mathbf{0} & 0 \end{bmatrix},$$

where $\mathbf{v} = -\boldsymbol{\omega} \times \mathbf{q}$, equation (2.5) can be rewritten as

$$\begin{bmatrix} \dot{\mathbf{r}}_k \\ 0 \end{bmatrix} = \begin{bmatrix} \hat{\boldsymbol{\omega}} & \mathbf{v} \\ \mathbf{0} & 0 \end{bmatrix} \begin{bmatrix} \mathbf{r}_k \\ 1 \end{bmatrix}.$$

Analogous to the definition of $\mathfrak{so}(3)$, we define [20]

$$\mathfrak{se}(3) = \{(\mathbf{v}, \hat{\boldsymbol{\omega}}) : \mathbf{v} \in \mathbb{R}^3, \hat{\boldsymbol{\omega}} \in \mathfrak{so}(3)\}. \quad (2.6)$$

The matrix $\hat{\boldsymbol{\xi}}$ is an element of $\mathfrak{se}(3)$ and it is referred to as a *twist* of the Euclidean group [20]. We use the operator \vee to define the 6-dimensional vector which parametrizes a *twist* [20],

$$\boldsymbol{\xi} = \begin{bmatrix} \hat{\boldsymbol{\omega}} & \mathbf{v} \\ \mathbf{0} & 0 \end{bmatrix}^{\vee} = \begin{bmatrix} \mathbf{v} \\ \boldsymbol{\omega} \end{bmatrix},$$

where $\boldsymbol{\omega}$ represents the rotational motion of \mathbf{r}_k and \mathbf{v} represents the translational motion of particle k .

2.1.4 Screw Theory

We use the geometrical concept of *screw* motion and *twist* to describe the trajectory into which we wish to stabilize a group of particles. In terms of screw theory [20], an element of $\mathfrak{se}(3)$ is called a twist [30].

Consider a particle on a trajectory that rotates by an angle θ about an axis parallel to the unit vector $\boldsymbol{\omega}$ and translates along the same axis by an amount d . This motion, which is reminiscent of the motion of a screw, defines screw motion and is depicted in Figure 2.2. The pitch, h , is the ratio of translational to rotational motion, i.e., $h = d/\theta$. The axis of rotation is $l = \{\mathbf{q} + \lambda\boldsymbol{\omega} : \lambda \in \mathbb{R}\}$, where \mathbf{q} is a point on axis l .

Definition 1. [20, Definition 2.2] *A screw consists of an axis l , a pitch h , and a magnitude M . A screw motion represents rotation by an amount $\theta = M$ about the*

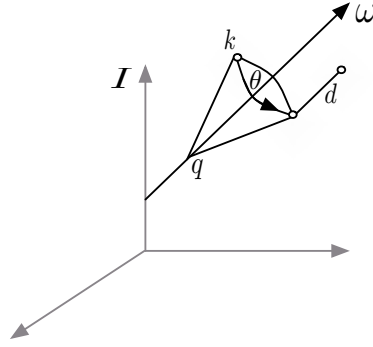


Figure 2.2: Schematic of screw motion.

axis l followed by translation by an amount $h\theta$ parallel to the axis l . If $h = \infty$ then the corresponding screw motion consists of a pure translation along the axis of the screw by a distance M .

The relations among the screw coordinates are

$$\begin{aligned}
 h &= \begin{cases} h = \frac{\boldsymbol{\omega}^T \mathbf{v}}{\|\boldsymbol{\omega}\|^2} & \text{if } \boldsymbol{\omega} \neq 0 \\ \infty & \text{if } \boldsymbol{\omega} = 0 \end{cases} \\
 l &= \begin{cases} \frac{\boldsymbol{\omega} \times \mathbf{v}}{\|\boldsymbol{\omega}\|^2} + \lambda \boldsymbol{\omega} & \text{if } \boldsymbol{\omega} \neq 0 \\ 0 + \lambda \boldsymbol{\omega} & \text{if } \boldsymbol{\omega} = 0 \end{cases} \\
 M &= \begin{cases} \|\boldsymbol{\omega}\| & \text{if } \boldsymbol{\omega} \neq 0 \\ \|\mathbf{v}\| & \text{if } \boldsymbol{\omega} = 0 \end{cases}
 \end{aligned}$$

In Chapter 3 we use screw coordinates to define the trajectory of a system of particles in three dimensions. If $\boldsymbol{\omega} \neq 0$ and the pitch $0 < h < 1$, helical trajectories are defined and if the pitch $h = 0$, circular trajectories are defined. If $\boldsymbol{\omega} = 0$, the pitch $h = \infty$ and parallel trajectories are defined.

2.2 Nonlinear Control Theory

We model different nonlinear systems and wish to study their behavior and stability. Nonlinear dynamical systems can be modeled as a system of coupled first-ordered differential equations [15]

$$\begin{aligned}\dot{x}_1 &= f_1(t, x_1, \dots, x_N, u_1, \dots, u_p) \\ \dot{x}_2 &= f_2(t, x_1, \dots, x_N, u_1, \dots, u_p) \\ &\vdots \\ \dot{x}_N &= f_N(t, x_1, \dots, x_N, u_1, \dots, u_p),\end{aligned}$$

where x_k , $k \in \{1, \dots, N\}$, are the state-variables, u_j , $j \in \{1, \dots, P\}$, are the control inputs, and t is time. This system of differential equations can be written in a more compact form. By writing the following vector notation,

$$x = \begin{bmatrix} x_1 \\ x_2 \\ \vdots \\ x_N \end{bmatrix}, \quad u = \begin{bmatrix} u_1 \\ u_2 \\ \vdots \\ u_P \end{bmatrix}, \quad f(t, x, u) = \begin{bmatrix} f_1(t, x, u) \\ f_2(t, x, u) \\ \vdots \\ f_N(t, x, u) \end{bmatrix},$$

we rewrite the system of differential equations as

$$\dot{x} = f(t, x, u),$$

This equation depends explicitly on time and is called non-autonomous or time-varying. Equations that do not depend explicitly on time are called autonomous or time-invariant, and are of the form

$$\dot{x} = f(x, u).$$

In this thesis we study both time-varying and time-invariant systems, and would like to know their behavior and stability of equilibrium points.

The concept of an equilibrium point plays an important role in the stability of dynamical systems. A point $x = x^*$ is an *equilibrium point* of $\dot{x} = f(t, x, u)$ if, whenever the state of the system starts near x^* , it remains near x^* for all time. A system can have one or multiple equilibrium points. We explain how to study the stability of equilibrium points for autonomous systems in Section 2.2.1 and for non-autonomous systems in Section 2.2.2.

2.2.1 Stability of Autonomous Systems

Consider the autonomous system

$$\dot{x} = f(x). \tag{2.7}$$

The origin $x^* = 0$ is an equilibrium point of (2.7) if

$$f(x^*) = 0.$$

Definition 2. [15, Definition 4.1] *The equilibrium point $x^* = 0$ of model (2.7) is*

- *stable if all solutions starting at nearby points stay nearby.*
- *unstable if it is not stable.*
- *asymptotically stable if it is stable and solutions tend to the equilibrium points as time approaches infinity, i.e., if we can choose an $\epsilon > 0$ such that*

$$\text{if } \|x(0)\| < \epsilon, \text{ then } \lim_{t \rightarrow \infty} x(t) = 0.$$

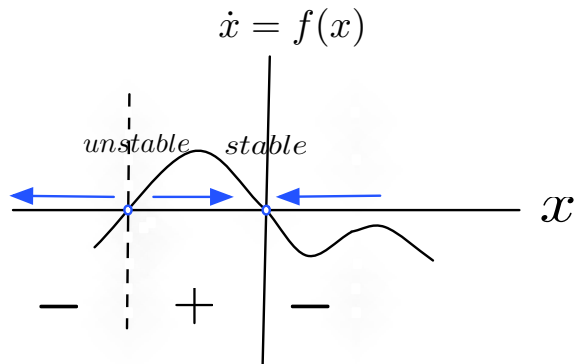


Figure 2.3: Example of the stability of an autonomous system.

A depiction of Definition 2 is shown in Figure 2.3. The system $\dot{x} = f(x)$ has two equilibrium points. A graphical method to determine the stability of the equilibrium points is to examine the variation in the sign of $f(x)$. We separate the function into segments between equilibrium points, drawing arrows to the left if $f(x)$ is negative and to the right if $f(x)$ is positive. The equilibrium point is unstable if both arrows face away from the point and stable if both arrows face toward the point.

Another method to determine the stability of an equilibrium point is to use Lyapunov's stability theorem:

Theorem 1. *Lyapunov Stability Theorem [15, Theorem 4.1]. Let $x^* = 0$ be an equilibrium point of (2.7) and $D \in \mathbb{R}^N$ be a domain containing $x^* = 0$. Let $V : D \rightarrow \mathbb{R}$ be a continuously differentiable function (called potential or Lyapunov function)*

such that

$$V(0) = 0 \text{ and } V(x) > 0 \in D - \{0\}$$

$$\dot{V} \leq 0 \in D.$$

Then x^* is stable. Also, if

$$\dot{V} < 0 \in D - \{0\},$$

then x^* is asymptotically stable.

Note that the time derivative of V is of the form

$$\dot{V}(x) = \sum_{i=1}^N \frac{\partial V}{\partial x_i} \dot{x}_i = \sum_{i=1}^N \frac{\partial V}{\partial x_i} f_i(x) = \begin{bmatrix} \frac{\partial V}{\partial x_1} & \dots & \frac{\partial V}{\partial x_N} \end{bmatrix} \begin{bmatrix} f_1(x) \\ \vdots \\ f_N(x) \end{bmatrix}.$$

It is important to keep in mind that Lyapunov functions are not unique. Therefore, failure of a Lyapunov function to satisfy the conditions for stability does not guarantee that an equilibrium point is unstable.

Definition 3. A potential function V is

- Positive definite if $V(0) = 0$ and $V(x) > 0 \forall x \neq 0$.
- Positive semi-definite if $V(0) = 0$ and $V(x) \geq 0 \forall x \neq 0$.
- Negative (semi-)definite if $-V(x)$ is positive (semi-)definite

Theorem 1 can also be stated as follows. The equilibrium point $x^* = 0$ is stable if there exists a continuously differentiable positive definite function $V(x)$ such that $\dot{V}(x)$ is negative semi-definite and $x^* = 0$ is asymptotically stable if $\dot{V}(x)$ is negative definite.

Sometimes it is not possible to show that an equilibrium point is asymptotically stable by using Theorem 1 because the potential function $V(x)$ might fail to be negative definite. In these cases, we use LaSalle's Invariance Principle. The following definitions are necessary.

Definition 4. [6] x_0 is a limit point of the set D if there exists a sequence in D which converges to x_0 .

Definition 5. [27] p is a positive limit point of $x(t)$, where $x(t)$ is a solution of (2.7), if there exists a sequence $\{t_n\}$, with $t_n \rightarrow \infty$ as $n \rightarrow \infty$, such that $x(t_n) \rightarrow p$ as $n \rightarrow \infty$. The set of all positive limit points of $x(t)$ is called the positive limit set of $x(t)$.

Definition 6. [27] The set M is invariant with respect to $\dot{x} = f(x)$ if, when $x(0) \in M$, $x(t) \in M \forall t \in \mathbb{R}$.

Theorem 2. LaSalle's Invariance Principle [15, Theorem 4.4]. Let $\Omega \subset D$ be a compact set that is positive invariant with respect to $\dot{x} = f(x)$. Let $V : D \rightarrow \mathbb{R}$ be a continuously differentiable function such that $\dot{V}(x) \leq 0 \in \Omega$. Let E be the set of all points in Ω where $\dot{V} = 0$. Let M be the largest invariant set in E . Then every solution starting in Ω approaches M as $t \rightarrow \infty$.

Note that unlike in Theorem 1, the function V does not have to be positive definite. It is also important to note that the invariance principle applies only to autonomous systems. Theorems 1 and 2 are used in Chapter 4 to prove the stability of the systems we are studying.

2.2.2 Stability of Non-autonomous Systems

Consider the time-varying system

$$\dot{x} = f(t, x), \tag{2.8}$$

The origin $x^* = 0$ is an equilibrium point of $\dot{x} = f(t, x)$ at $t = 0$ if

$$f(t, 0) = 0 \quad \forall t \geq 0.$$

To prove the stability of x^* in model (2.8), we use the following invariance-like theorem adapted for time-varying systems.

Theorem 3. *[15, Theorem 8.4] Let $D \in \mathbb{R}^n$ be a domain containing $x = 0$ and suppose $f(x, t)$ is piecewise continuous in t and locally Lipschitz in x , uniformly in t , on $[0, \infty) \times D$. Furthermore, suppose $f(0, t)$ is uniformly bounded for all $t \geq 0$. Let $V : [0, \infty) \times D \rightarrow \mathbb{R}$ be a continuously differentiable function such that*

$$W_1(x) \leq V(x, t) \leq W_2(x)$$

$$\dot{V}(x, t) = \frac{\partial V}{\partial t} + \frac{\partial V}{\partial x} f(x, t) \leq W(x)$$

$\forall t \geq 0, \forall x \in D$, where $W_1(x)$ and $W_2(x)$ are continuous positive definite functions and $W(x)$ is a continuous positive semidefinite function on D . Choose $r > 0$ such that $B_r \subset D$ and let $\rho < \min_{\|x\|=r} W_1(x)$. Then, all solutions of $\dot{x} = f(x, t)$ with $x(t_0) \in \{x \in B_r | W_2(x) \leq \rho\}$ are bounded and satisfy

$$W(x(t)) \rightarrow 0 \text{ as } t \rightarrow \infty.$$

Moreover, if all the assumptions hold globally and $W_1(x)$ is radially unbounded, the statement is true for all $x(t_0) \in \mathbb{R}^n$.

The limit $W(x(t)) \rightarrow 0$ implies that $x(t)$ approaches E as $t \rightarrow \infty$, where

$$E = \{x \in D | W(x) = 0\}.$$

Theorem 3 is used in Chapter 4 to prove the stability of the systems we are studying.

2.3 Graph Theory

To design control laws that stabilize a group of unmanned vehicles, it is necessary to know how information flows throughout the group. Graph theory is used to demonstrate how individuals in the group communicate with one another.

2.3.1 Directed vs. Undirected Graphs

We model the information flow by means of a graph. The agents are assumed to be connected and fully actuated, but the information they can obtain might be limited. There are two types of graphs: directed and undirected. A directed graph is one in which each agent $k \in \{1, \dots, N\}$ only gets information from a subset of other agents $j \neq k$; that is, $j \rightarrow k$. On the other hand, a graph is undirected, or bidirectional, if $j \rightarrow k$ whenever $k \rightarrow j$ (see Figure 2.4). We use a communication topology that is undirected and time-invariant, though this can be extended to directed, time-varying topologies [34].

2.3.2 Laplacian Matrix

The communication network is depicted by the Laplacian matrix L . A graph $G = (N, E)$ has N vertices, where N is the number of agents, E is the set of edges,

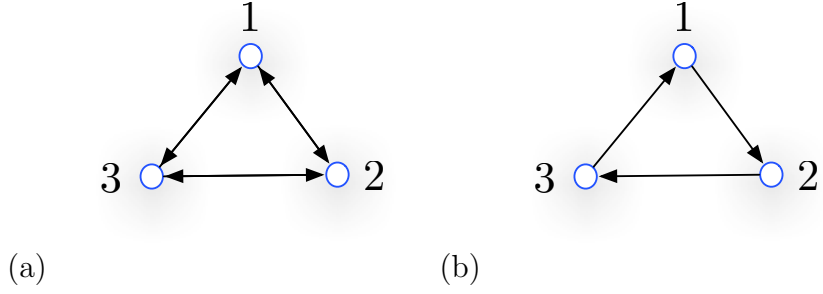


Figure 2.4: Example of (a) an undirected and (b) a directed graph.

and L is a matrix formed with the sum of binary components a_{kj} which represent the existence of information flow from j to k , $k \in \{1, \dots, N\}$. If there is communication, then $a_{kj} = 1$, otherwise, $a_{kj} = 0$. The Laplacian matrix L is

$$l_{kj} = \begin{cases} \sum_i a_{ki} & \text{if } j = k \\ -a_{kj} & \text{if } (j, k) \in E \\ 0 & \text{otherwise.} \end{cases}$$

It is an $N \times N$ matrix and has the property that the sum of each row is equal to zero; that is, $L\mathbf{1} = \mathbf{0}$, where $\mathbf{1}$ is an $N \times 1$ column vector, whose entries are all 1. If G is connected and undirected then the null space of L is spanned by $\mathbf{1}$.

In some cases throughout the thesis we add a “virtual” agent to the system in order to augment a control law to obtain a formation in a desired location or direction. To do this, we augment the communication graph by an additional reference node 0, with directed edges from 0 to the informed agents. In this case we define $G_0 = (\mathcal{N}_0, E_0)$ to be a time-invariant and rooted graph, where $\mathcal{N}_0 = \{0, 1, \dots, N\}$,

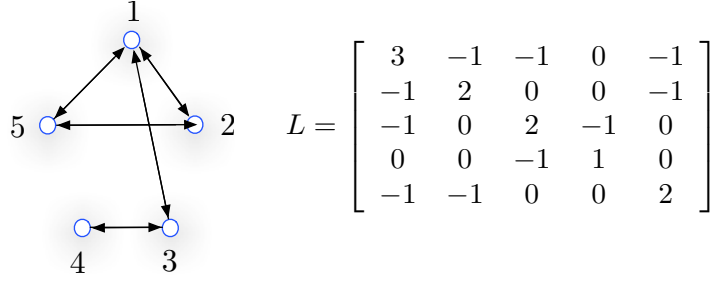


Figure 2.5: Example of undirected communication topology with 5 agents

and L_0 is the Laplacian matrix of the form [34]

$$L_0 = \left[\begin{array}{c|c} 0 & 0 \cdots 0 \\ \hline -a_{10} & \\ \vdots & L - \text{diag} \{-a_{k0}\} \\ -a_{N0} & \end{array} \right],$$

where $-a_{k0} \in k = \{1, \dots, N\}$ represent information transmitted from the virtual agent to particle k .

We use the Kronecker product to define the matrix $\mathcal{L} \triangleq L \otimes I_3$, which is used in the control laws derived in Chapter 4. We will also use \mathcal{L}_k , $k \in \{1, \dots, N\}$, which denote three consecutive rows of \mathcal{L} starting with row $3k - 2$.

To help understand how to construct a Laplacian matrix, Figure 2.5 shows an example of an undirected, connected, and time-invariant graph with $N = 5$.

Chapter 3

Particle Dynamics in a Time-Varying Flowfield

This chapter is dedicated to deriving the dynamics of a group of N self-propelled particles traveling in three dimensions in a time-varying flowfield. We model the system in three dimensions in Section 3.1. In Section 3.2, we constrain the particles to travel on the surface of a rotating sphere in a time-varying flowfield.

3.1 Particle Motion in Three Dimensions

The model studied in this section introduces a three-dimensional, time-varying flowfield to the flow-free model described in [14] and further studied in [30]. The flow-free model is summarized in Section 3.1.1. In Section 3.1.2 we derive the particle dynamics in a time-varying flowfield.

3.1.1 Flow-Free Particle Dynamics

The flow-free model consists of N identical particles moving at unit speed in three dimensions as shown in Figure 3.1(a). The position of particle $k \in \{1, \dots, N\}$ is represented by $\mathbf{r}_k \in \mathbb{R}^3$ and its velocity relative to an inertial frame \mathcal{I} by $\dot{\mathbf{r}}_k$. Control $\mathbf{u}_k = [w_k \ -h_k \ q_k]^T \in \mathbb{R}^3$ steers each particle by rotating its velocity about the unit vectors of a path frame, $\mathcal{C}_k = (k, \mathbf{x}_k, \mathbf{y}_k, \mathbf{z}_k)$, which is fixed to particle k such that the unit vector \mathbf{x}_k points in the direction of the velocity of particle k . (\mathcal{C}_k is

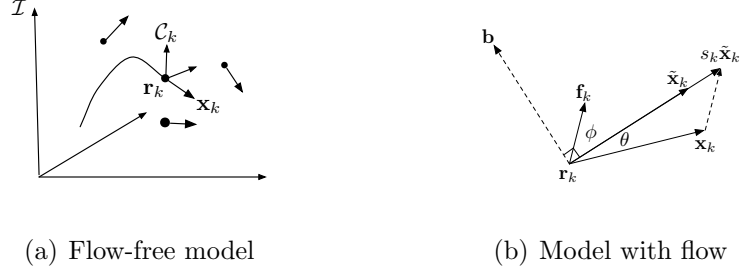


Figure 3.1: Schematic of vectors used in the three-dimensional motion models. (a) In the flow-free model (3.1), path frame \mathcal{C}_k is aligned with the velocity of particle k relative to an inertial frame \mathcal{I} . (b) In the model (3.3) with flow $\mathbf{f}_k(t)$, the inertial velocity of particle k is $\mathbf{x}_k + \mathbf{f}_k(t) = s_k \tilde{\mathbf{x}}_k$ (not used until Section 3.1.2).

a right-handed reference frame and $\mathbf{x}_k, \mathbf{y}_k$, and $\mathbf{z}_k \in \mathbb{R}^3$.) The equations of motion are [14]

$$\begin{aligned}
 \dot{\mathbf{r}}_k &= \mathbf{x}_k \\
 \dot{\mathbf{x}}_k &= q_k \mathbf{y}_k + h_k \mathbf{z}_k \\
 \dot{\mathbf{y}}_k &= -q_k \mathbf{x}_k + w_k \mathbf{z}_k \\
 \dot{\mathbf{z}}_k &= -h_k \mathbf{x}_k - w_k \mathbf{y}_k,
 \end{aligned} \tag{3.1}$$

where q_k (resp. h_k) represents the curvature control of the k th particle about the \mathbf{y}_k (resp. \mathbf{z}_k) axis. The torsion control w_k allows the velocity of particle k to rotate about the \mathbf{x}_k axis.

The dynamics in (3.1) represent a control system on the Lie group $SE(3)$ (see Section 2.1.3) [14, 30] and, consequently, can be expressed in terms of the group variable

$$g_k = \begin{bmatrix} R_k & \mathbf{r}_k \\ \mathbf{0} & 1 \end{bmatrix} \in SE(3),$$

where $R_k = [\mathbf{x}_k \ \mathbf{y}_k \ \mathbf{z}_k]$. The dynamics (3.1) are equivalent to $\dot{g}_k = g_k \hat{\xi}_k$, where

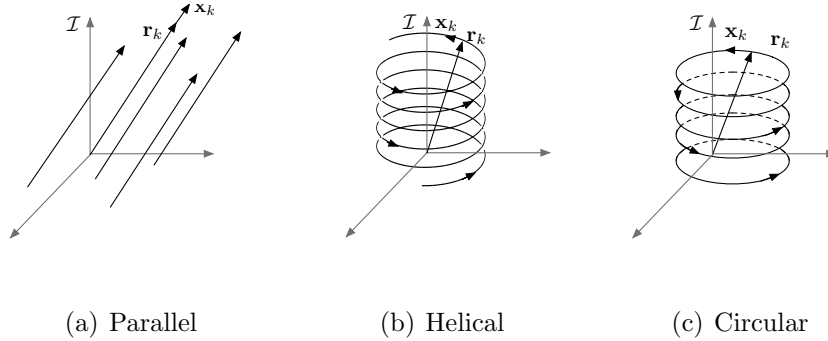


Figure 3.2: Schematic of *relative equilibria* of model (3.1) [14, 31]. Control algorithms to obtain these formations in a time-varying flow are derived in Sections 4.1 and 4.2.

$\hat{\xi}_k \in \mathfrak{se}(3)$ is an element of the Lie algebra of $SE(3)$,

$$\hat{\xi}_k = \begin{bmatrix} \hat{\mathbf{u}}_k & \mathbf{e}_1 \\ \mathbf{0} & 0 \end{bmatrix},$$

and $\mathbf{e}_1 = [1 \ 0 \ 0]^T$. $\hat{\mathbf{u}}_k$ is the 3×3 skew-symmetric matrix that represents an element of $\mathfrak{so}(3)$, the Lie algebra of $SO(3)$ (see Section 2.1.2).

The closed-loop dynamics of model (3.1) are invariant under rigid motions in $SE(3)$ provided the controls \mathbf{u}_k depend only on *shape* variables—relative positions and relative orientations of the path frames \mathcal{C}_k , $k \in \{1, \dots, N\}$. In this case, a special set of solutions of the closed-loop dynamics correspond to steady-state formations, called *relative equilibria* [14, 30], in which the position and path-frame orientation of particle k *relative* to the position and path-frame orientation of particle $j \neq k$ is fixed. The three types of *relative equilibria* of model (3.1) are sketched in Figure 3.2 [14]: parallel, helical, and circular motions. Algorithms to stabilize these

formations in the flow-free model (3.1) are provided in [31]. We provide algorithms to stabilize these types of formations in a three-dimensional, time-varying flowfield in Sections 4.1 and 4.2.

3.1.2 Particle Dynamics in a Time-Varying Flowfield

In this section, we introduce a model of N particles traveling in a three-dimensional flowfield \mathbf{f} that varies in space and time. The instantaneous velocity of the flow at \mathbf{r}_k is denoted by $\mathbf{f}_k(t) = \mathbf{f}(\mathbf{r}_k, t)$. Expressed in vector components with respect to the path frame C_k , the flow is

$$\mathbf{f}_k(t) = p_k(t)\mathbf{x}_k + t_k(t)\mathbf{y}_k + v_k(t)\mathbf{z}_k,$$

where the time-varying coefficients are $p_k(t) = \mathbf{f}_k(t) \cdot \mathbf{x}_k$, $t_k(t) = \mathbf{f}_k(t) \cdot \mathbf{y}_k$, and $v_k(t) = \mathbf{f}_k(t) \cdot \mathbf{z}_k$. We assume that the flow satisfies the following three assumptions:

- A1) The components of $\mathbf{f}_k(t)$ expressed in C_k are known by particle k at time t .
- A2) The flow speed is less than the particle speed relative to the flow, i.e., $\|\mathbf{f}_k(t)\| < 1 \forall k, t$.
- A3) $\mathbf{f}_k(t)$ is differentiable in \mathbf{r}_k and t .

Assumption A2 ensures that a particle can always make forward progress as measured from an inertial frame. The inertial velocity of particle k is the sum of its velocity relative to the flow and the velocity of the flow, i.e.,

$$\dot{\mathbf{r}}_k = \mathbf{x}_k + \mathbf{f}_k(t) = (1 + p_k(t))\mathbf{x}_k + t_k(t)\mathbf{y}_k + v_k(t)\mathbf{z}_k. \quad (3.2)$$

We associate frame \mathcal{C}_k with motion relative to the flowfield by expressing the dynamics (3.1) with $\dot{\mathbf{r}}_k$ given by (3.2) using a second path frame, $\mathcal{D}_k = (k, \tilde{\mathbf{x}}_k, \tilde{\mathbf{y}}_k, \tilde{\mathbf{z}}_k)$, which is aligned with the *inertial* velocity of particle k , i.e., $\tilde{\mathbf{x}}_k$ is parallel to $\dot{\mathbf{r}}_k$ (see Figure 3.1(b)). Let $s_k(t) = \|\mathbf{x}_k + \mathbf{f}_k(t)\|$ denote the (time-varying) inertial speed of particle k . The dynamics expressed as components in frame \mathcal{D}_k are

$$\begin{aligned}\dot{\mathbf{r}}_k &= s_k(t)\tilde{\mathbf{x}}_k \\ \dot{\tilde{\mathbf{x}}}_k &= \tilde{q}_k\tilde{\mathbf{y}}_k + \tilde{h}_k\tilde{\mathbf{z}}_k \\ \dot{\tilde{\mathbf{y}}}_k &= -\tilde{q}_k\tilde{\mathbf{x}}_k + \tilde{w}_k\tilde{\mathbf{z}}_k \\ \dot{\tilde{\mathbf{z}}}_k &= -\tilde{h}_k\tilde{\mathbf{x}}_k - \tilde{w}_k\tilde{\mathbf{y}}_k,\end{aligned}\tag{3.3}$$

where $\tilde{\mathbf{u}}_k = [\tilde{w}_k \ -\tilde{h}_k \ \tilde{q}_k]^T$ are the steering controls relative to frame \mathcal{D}_k . Note that the dynamics in (3.3) still represent a control system on $\text{SE}(3)$, since

$$\dot{\hat{\mathbf{g}}}_k = \tilde{g}_k \hat{\xi}_k = \begin{bmatrix} \tilde{R}_k & \mathbf{r}_k \\ \mathbf{0} & 1 \end{bmatrix} \begin{bmatrix} \hat{\mathbf{u}}_k & s_k(t)\mathbf{e}_1 \\ \mathbf{0} & 0 \end{bmatrix},$$

where $\tilde{R}_k = [\tilde{\mathbf{x}}_k \ \tilde{\mathbf{y}}_k \ \tilde{\mathbf{z}}_k]$ and $\hat{\mathbf{u}} \in \mathfrak{se}(3)$. We will make use of the fact that (3.3) implies

$$\dot{\tilde{\mathbf{x}}}_k = \tilde{R}_k \tilde{\mathbf{u}}_k \times \tilde{\mathbf{x}}_k.\tag{3.4}$$

To define parallel and helical formations in three dimensions we use the concept of *twist* [30], which is related to screw motion [20] (see Section 2.1.4). We use the operator \vee to find a 6-dimensional vector which parametrizes a *twist* of the matrix $\hat{\xi}_k$ [20],

$$\tilde{\xi}_k = \hat{\xi}_k^\vee = \begin{bmatrix} \hat{\mathbf{u}}_k & s_k(t)\mathbf{e}_1 \\ \mathbf{0} & 0 \end{bmatrix}^\vee = \begin{bmatrix} s_k(t)\mathbf{e}_1 \\ \tilde{\mathbf{u}}_k \end{bmatrix} \in \mathbb{R}^6.\tag{3.5}$$

A constant screw motion is defined by the constant *twist* $\tilde{\boldsymbol{\xi}}_0 = [\tilde{\mathbf{v}}_0^T, \boldsymbol{\omega}_0^T]^T \in \mathbb{R}^6$ [20].

When $\boldsymbol{\omega}_0 \neq 0$, the motion is defined by a rotation about an axis parallel to $\boldsymbol{\omega}_0$.

When $\boldsymbol{\omega}_0 = 0$, the motion is defined by a pure translation along the axis \mathbf{v}_0 . The

pitch α_0 is the ratio of translational to rotational motion and its value in constant motion is [20]

$$\alpha_0 = \begin{cases} \frac{\boldsymbol{\omega}_0^T \mathbf{v}_0}{\|\boldsymbol{\omega}_0\|^2}, & \text{if } \boldsymbol{\omega}_0 \neq 0 \\ \infty, & \text{if } \boldsymbol{\omega}_0 = 0 \end{cases}$$

Following [30], we define a helical trajectory with the following consensus variable¹:

$$\tilde{\mathbf{v}}_k^a = \tilde{\mathbf{x}}_k + \mathbf{r}_k \times \boldsymbol{\omega}_0, \quad \boldsymbol{\omega}_0 \neq 0. \quad (3.6)$$

Using (3.4), the velocity of $\tilde{\mathbf{v}}_k^a$ along solutions of (3.3) is $\dot{\tilde{\mathbf{v}}}_k^a = \left(\tilde{R}_k \tilde{\mathbf{u}}_k - s_k(t) \boldsymbol{\omega}_0 \right) \times \tilde{\mathbf{x}}_k$. The following extends [30, Proposition 1] to helical motion in a time-varying flowfield.

Lemma 1. *Let $\mathbf{f}_k(t) = \mathbf{f}(\mathbf{r}_k, t)$ be a three-dimensional, time-varying flowfield that satisfies assumptions A1–A3. The control $\tilde{\mathbf{u}}_k = \tilde{R}_k^T s_k(t) \boldsymbol{\omega}_0$ steers particle k in model (3.3) around a helix with axis of rotation parallel to $\boldsymbol{\omega}_0$, radius $\|\boldsymbol{\omega}_0\|^{-1}$, and pitch $\alpha_k = \tilde{\mathbf{x}}_k \cdot \boldsymbol{\omega}_0 / \|\boldsymbol{\omega}_0\|^2$, such that $\tilde{\mathbf{v}}_k^a$ is fixed, i.e., $\dot{\tilde{\mathbf{v}}}_k^a = 0$, where $\tilde{\mathbf{v}}_k^a$ is defined in (3.6). A helical formation of N particles is characterized by the condition $\tilde{\mathbf{v}}_k^a = \tilde{\mathbf{v}}_j^a$ for all pairs $j, k \in \{1, \dots, N\}$.*

Proof. $\tilde{\mathbf{v}}_k^a$ is constant because when substituting $\tilde{\mathbf{u}}_k = \tilde{R}_k^T s_k(t) \boldsymbol{\omega}_0$ into $\dot{\tilde{\mathbf{v}}}_k^a$ yields $\dot{\tilde{\mathbf{v}}}_k^a = \left(\tilde{R}_k \tilde{\mathbf{u}}_k - s_k(t) \boldsymbol{\omega}_0 \right) \times \tilde{\mathbf{x}}_k = (s_k(t) \boldsymbol{\omega}_0 - s_k(t) \boldsymbol{\omega}_0) \times \tilde{\mathbf{x}}_k = \mathbf{0}$. Using (3.5), the

¹The superscript a indicates that the vector components are expressed in a fixed (inertial) reference frame.

instantaneous pitch of particle k is

$$\alpha_k = \frac{s_k \mathbf{e}_1^T \tilde{\mathbf{u}}_k}{\|\tilde{\mathbf{u}}_k\|^2} \Big|_{\tilde{\mathbf{u}}_k = \tilde{R}_k^T s_k(t) \boldsymbol{\omega}_0} = \frac{\tilde{\mathbf{x}}_k \cdot \boldsymbol{\omega}_0}{\|\boldsymbol{\omega}_0\|^2} \leq 1,$$

which is also constant since

$$\frac{d}{dt} \left(\frac{\tilde{\mathbf{x}}_k \cdot \boldsymbol{\omega}_0}{\|\boldsymbol{\omega}_0\|^2} \right) \Big|_{\dot{\tilde{\mathbf{x}}}_k = s_k(t) \boldsymbol{\omega}_0 \times \tilde{\mathbf{x}}_k} = \frac{s_k(t) \boldsymbol{\omega}_0 \times \tilde{\mathbf{x}}_k \cdot \boldsymbol{\omega}_0}{\|\boldsymbol{\omega}_0\|^2} = 0.$$

□

A circular trajectory can be described as a helical trajectory with zero pitch. A parallel trajectory can be described as a helical trajectory with infinite pitch, for example when $\boldsymbol{\omega}_0 = 0$. The following extends [30, Proposition 1] to parallel motion in a time-varying flowfield.

Lemma 2. *Let $\mathbf{f}_k(t) = \mathbf{f}(\mathbf{r}_k, t)$ be a three-dimensional, time-varying flowfield that satisfies assumptions A1–A3. The control $\tilde{\mathbf{u}}_k = 0$ steers particle k in model (3.3) in a straight line such that $\tilde{\mathbf{x}}_k$ is fixed, i.e., $\dot{\tilde{\mathbf{x}}}_k = 0$. A parallel formation is characterized by the condition $\tilde{\mathbf{x}}_k = \tilde{\mathbf{x}}_j$ for all pairs $j, k \in \{1, \dots, N\}$.*

Transformation Between Relative and Inertial Path Frames: Using (3.2) and (3.3), we have

$$\tilde{\mathbf{x}}_k = \frac{1 + p_k(t)}{s_k(t)} \mathbf{x}_k + \frac{t_k(t)}{s_k(t)} \mathbf{y}_k + \frac{v_k(t)}{s_k(t)} \mathbf{z}_k. \quad (3.7)$$

We use (3.7) to derive the relationship between frames \mathcal{C}_k and \mathcal{D}_k . This relationship is important because we design the steering controls $\tilde{\mathbf{u}}_k$ using (3.3) and the platform dynamics are presumed to obey (3.1). Thus it is important in applications to be able to find \mathbf{u}_k in terms of $\tilde{\mathbf{u}}_k$ and $\mathbf{f}_k(t)$. The transformation between the \mathcal{C}_k and

\mathcal{D}_k frames and an analytical expression for each component of \mathbf{u}_k in terms of the components of $\tilde{\mathbf{u}}_k$ and $\mathbf{f}_k(t)$ are provided in Appendix A.

Inertial speed in a three-dimensional flowfield: Unlike in the flow-free model (3.1), the inertial speed $s_k(t)$ of particle k in model (3.3) is not constant—it depends on the flow and the direction of motion. Using (3.7), the inertial speed of particle k is

$$s_k(t) = \|\dot{s}_k(t)\tilde{\mathbf{x}}_k\| = \sqrt{(1 + p_k(t))^2 + t_k^2(t) + v_k^2(t)} > 0,$$

where $p_k(t)$, $t_k(t)$, and $v_k(t)$ are components of $\mathbf{f}_k(t)$ in frame \mathcal{C}_k . However, in order to integrate (3.3), we need an expression for $s_k(t)$ in terms of the components of $\mathbf{f}_k(t)$ in frame \mathcal{D}_k .

Theorem 4. *Let $\mathbf{f}_k(t) = \mathbf{f}(\mathbf{r}_k, t)$ be a three-dimensional, time-varying flowfield that satisfies assumptions A1–A3. The inertial speed of particle k in model (3.3) is*

$$s_k(t) = \sqrt{1 - \|\tilde{\mathbf{x}}_k \times \mathbf{f}_k(t)\|^2 + \tilde{\mathbf{x}}_k \cdot \mathbf{f}_k(t)}. \quad (3.8)$$

The proof of Theorem 4 is provided in Appendix B. Note, (3.8) is used to integrate (3.3) and only requires knowledge of $\mathbf{f}_k(t)$ expressed in \mathcal{D}_k . However, to compute \mathbf{u}_k from $\tilde{\mathbf{u}}_k$, we need to know $\mathbf{f}_k(t)$ in \mathcal{C}_k .

3.2 Particle Motion on a Rotating Sphere

We now constrain particle motion in the three-dimensional model to the surface of a sphere. The model studied here extends the spherical model introduced in [24], which consists of N identical particles moving at a constant speed on the surface

of a non-rotating sphere in a flow-free environment. This model is summarized in Section 3.2.1. We expand this framework by introducing rotation to the sphere (derived in Section 3.2.2) and adding a time-varying flowfield to the model (derived in Section 3.2.3).

3.2.1 Flow-Free Particle Dynamics

The flow-free model consists of N particles moving at unit speed on the surface of a sphere with radius $\rho_0 > 0$ and center O . The position of particle $k \in \{1, \dots, N\}$ relative to O is represented by $\mathbf{r}_k \in \mathbb{R}^3$ (see Figure 3.3(a)). A path frame $\mathcal{C}_k = (k, \mathbf{x}_k, \mathbf{y}_k, \mathbf{z}_k)$ is fixed to particle k such that the unit vector \mathbf{x}_k points in the direction of the velocity of particle k , \mathbf{z}_k is orthogonal to the sphere at \mathbf{r}_k , and \mathbf{y}_k completes the right-handed reference frame. Note \mathbf{z}_k is the unit vector of the position \mathbf{r}_k , i.e., $\mathbf{r}_k = \rho_0 \mathbf{z}_k$.

A gyroscopic force steers each particle k on the surface of the sphere. This force is modeled as a state-feedback control u_k that rotates the velocity of each particle about \mathbf{z}_k . The equations of motion are [24]

$$\begin{aligned}
 \dot{\mathbf{r}}_k &= \mathbf{x}_k \\
 \dot{\mathbf{x}}_k &= u_k \mathbf{y}_k - \rho_0^{-1} \mathbf{z}_k \\
 \dot{\mathbf{y}}_k &= -u_k \mathbf{x}_k \\
 \dot{\mathbf{z}}_k &= \rho_0^{-1} \mathbf{x}_k.
 \end{aligned} \tag{3.9}$$

The relationship between (3.9) and (3.1) can be found by substituting $\mathbf{u}_k = [0 \ 0 \ u_k]^T$ into (3.1) and taking into account the radius of the sphere in the dynamics. Note that the dynamics in (3.9) represent a control system on the Lie group $SE(3)$ [14, 32].

Alternatively, since \mathbf{r}_k is parallel to \mathbf{z}_k , the dynamics evolve on $SO(3)$ according to

$$\dot{R}_k = R_k \hat{\boldsymbol{\eta}}_k = \begin{bmatrix} \mathbf{x}_k & \mathbf{y}_k & \mathbf{z}_k \end{bmatrix} \begin{bmatrix} 0 & -u_k & s_0 \\ u_k & 0 & 0 \\ -s_0 & 0 & 0 \end{bmatrix},$$

where $\hat{\boldsymbol{\eta}}_k \in \mathfrak{so}(3)$ is a skew-symmetric matrix (see Section 2.1.2).

The force, \mathbf{F}_k , on particle k is the sum of the constraint (normal) force N_k that acts orthogonally to the surface of the sphere and the gyroscopic (steering) force u_k that acts tangentially to the surface of the sphere and orthogonally to \mathbf{x}_k , i.e.,

$$\mathbf{F}_k = -N_k \mathbf{z}_k + u_k \mathbf{y}_k, \quad (3.10)$$

where we assume the particles have unit mass.

3.2.2 Particle Dynamics on a Rotating Sphere

We extend the framework described in [24] by adding rotation to the sphere, which introduces a Coriolis effect. Coriolis acceleration contributes to the apparent deflection of each particle when viewed from a frame fixed to the sphere, and is given by $\mathbf{a}_k^{cor} = -2\boldsymbol{\omega}_1 \times \dot{\mathbf{r}}_k$, where $\boldsymbol{\omega}_1$ is the angular velocity vector of the sphere and $\dot{\mathbf{r}}_k$ is the velocity relative to the (moving) surface of the sphere [1]².

In order to derive the particle dynamics on a rotating sphere, we use a spherical coordinate system consisting of the azimuth angle θ_k , the polar angle ϕ_k and the (fixed) radius ρ_0 . An inertial reference frame \mathcal{I} is defined by $\mathcal{I} = (O, \mathbf{e}_x, \mathbf{e}_y, \mathbf{e}_z)$,

²In this section, we derive the dynamics on a rotating sphere, starting with $\mathbf{a}_k^{cor} = -2\boldsymbol{\omega}_1 \times \dot{\mathbf{r}}_k$.

For the full proof, refer to Appendix C.

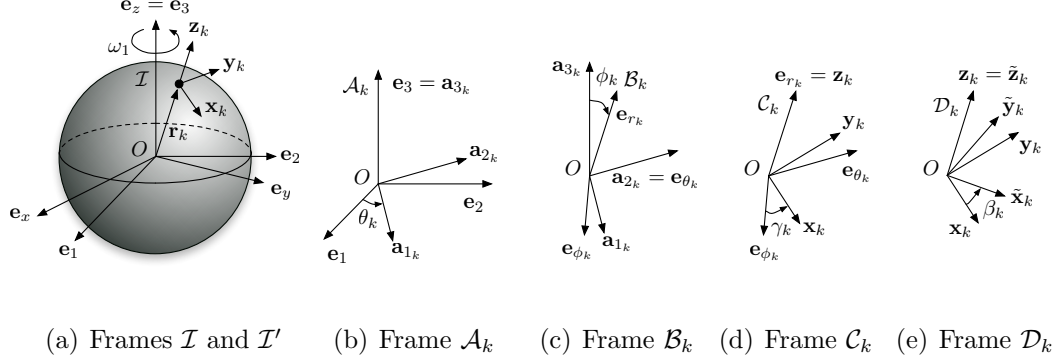


Figure 3.3: Reference frames used to derive particle dynamics on the sphere. Each frame differs from the previous one by a simple rotation. Note that frame \mathcal{D}_k is not used until Section 3.2.3.

where the origin O is located at the center of the sphere and \mathbf{e}_x , \mathbf{e}_y , and \mathbf{e}_z are unit vectors (see Figure 3.3). We assume that $\boldsymbol{\omega}_1$ is aligned with \mathbf{e}_z , so that the sphere rotates at constant angular rate ω_1 about \mathbf{e}_z .

We introduce four additional reference frames. Frame $\mathcal{I}' = (O, \mathbf{e}_1, \mathbf{e}_2, \mathbf{e}_3)$ is fixed to the sphere and differs from \mathcal{I} by a rotation of $\omega_1 t$ about $\mathbf{e}_3 = \mathbf{e}_z$, where t is time. Frame $\mathcal{A}_k = (O, \mathbf{a}_{1k}, \mathbf{a}_{2k}, \mathbf{a}_{3k})$, $k \in \{1, \dots, N\}$, differs from \mathcal{I} by a rotation of θ_k about $\mathbf{a}_{3k} = \mathbf{e}_3$. Frame $\mathcal{B}_k = (O, \mathbf{e}_{\phi_k}, \mathbf{e}_{\theta_k}, \mathbf{e}_{r_k})$ —the spherical body frame—differs from \mathcal{A}_k by a rotation of ϕ_k about $\mathbf{e}_{\theta_k} = \mathbf{a}_{2k}$. The unit vector \mathbf{e}_{r_k} points from O to the position \mathbf{r}_k of particle k . The fourth frame, $\mathcal{C}_k = (k, \mathbf{x}_k, \mathbf{y}_k, \mathbf{z}_k)$, differs from \mathcal{B}_k by a rotation of the orientation angle γ_k about $\mathbf{z}_k = \mathbf{e}_{r_k}$. The origin of \mathcal{C}_k is attached to particle k and the unit vector \mathbf{x}_k points in the direction of motion of particle k relative to the sphere-fixed frame \mathcal{I}' .

The unit vectors of the four non-inertial reference frames are related by the

following transformation table³

	\mathbf{e}_1	\mathbf{e}_2	\mathbf{e}_3	\mathbf{e}_{ϕ_k}	\mathbf{e}_{θ_k}	\mathbf{e}_{r_k}
\mathbf{a}_{1_k}	$\cos \theta_k$	$\sin \theta_k$	0	$\cos \phi_k$	0	$\sin \phi_k$
\mathbf{a}_{2_k}	$-\sin \theta_k$	$\cos \theta_k$	0	0	1	0
\mathbf{a}_{3_k}	0	0	1	$-\sin \phi_k$	0	$\cos \phi_k$
\mathbf{x}_k	*	*	*	$\cos \gamma_k$	$\sin \gamma_k$	0
\mathbf{y}_k	*	*	*	$-\sin \gamma_k$	$\cos \gamma_k$	0
\mathbf{z}_k	*	*	*	0	0	1

The angular velocity ${}^{\mathcal{I}}\boldsymbol{\omega}^{\mathcal{C}_k}$ of frame \mathcal{C}_k with respect to the inertial frame \mathcal{I} is ${}^{\mathcal{I}}\boldsymbol{\omega}^{\mathcal{C}_k} = (\omega_1 + \dot{\theta}_k)\mathbf{a}_{3_k} + \dot{\phi}_k\mathbf{e}_{\theta_k} + \dot{\gamma}_k\mathbf{z}_k$, where $\mathbf{a}_{3_k} = -\sin \phi_k\mathbf{e}_{\phi_k} + \cos \phi_k\mathbf{e}_{r_k} = -\sin \phi_k \cos \gamma_k\mathbf{x}_k + \sin \phi_k \sin \gamma_k\mathbf{y}_k + \cos \phi_k\mathbf{z}_k$ and $\mathbf{e}_{\theta_k} = \sin \gamma_k\mathbf{x}_k + \cos \gamma_k\mathbf{y}_k$ are found from the transformation table.

The inertial acceleration due to the Coriolis effect is

$$\mathbf{a}_k^{cor} = -2{}^{\mathcal{I}}\boldsymbol{\omega}^{\mathcal{C}_k} \times \dot{\mathbf{r}}_k = -2\omega_1 \cos \phi_k \mathbf{y}_k + 2\omega_1 \sin \gamma_k \mathbf{z}_k. \quad (3.11)$$

The Coriolis acceleration contributes a fictional force, \mathbf{F}_k^{cor} , that acts on particle k .

Combining (3.10) and (3.11), we obtain

$$\mathbf{F}_k + \mathbf{F}_k^{cor} = (2\omega_1 \sin \gamma_k - N_k) \mathbf{z}_k + (u_k - 2\omega_1 \cos \phi_k) \mathbf{y}_k. \quad (3.12)$$

Comparing the \mathbf{y}_k components of (3.10) and (3.12), we observe that the control u_k is augmented by $-2\omega_1 \cos \phi_k$. Since $\cos \phi_k = \mathbf{z}_k \cdot \mathbf{e}_3 = z_{k3}$ from the transformation table, we define the effective control [8]

$$\nu_k = u_k - 2\omega_1 z_{k3}, \quad (3.13)$$

³Entries marked * can be computed from the other entries.

where $-2\omega_1 z_{k3}$ appears due to the Coriolis effect (for the full proof, refer to Appendix C). Under the effective control (3.13), the dynamics of particle k relative to the sphere-fixed frame \mathcal{I}' are

$$\begin{aligned}
\dot{\mathbf{r}}_k &= \mathbf{x}_k \\
\dot{\mathbf{x}}_k &= \nu_k \mathbf{y}_k - \rho_0^{-1} \mathbf{z}_k \\
\dot{\mathbf{y}}_k &= -\nu_k \mathbf{x}_k \\
\dot{\mathbf{z}}_k &= \rho_0^{-1} \mathbf{x}_k.
\end{aligned} \tag{3.14}$$

Thus, if we use (3.14) to design ν_k , then use (3.13) to compute u_k , the Coriolis effect will be cancelled.

The closed-loop dynamics (3.14) possess only one of the three types of *relative equilibria* described in Section 3.1.1: circular motion with a common radius, axis of rotation, and direction of rotation [24]. This *relative equilibrium* is formed by the intersection of the sphere and a cylinder of radius $\rho'_0 \leq \rho_0$ whose longitudinal axis passes through the center of the sphere. If $\rho'_0 < \rho_0$, the particles will travel around either one of two circles on opposite sides of the sphere (see Figure 3.4(a)). Algorithms to stabilize circular formations in the flow-free model (3.9) are provided in [24]. We provide algorithms to stabilize circular formations in a time-varying flowfield on a rotating sphere in Section 4.3.

A circular trajectory on the surface of a sphere can also be described as the intersection of the sphere and a right circular cone whose axis of rotation passes through the center of the sphere and whose apex is outside the sphere (see Figure

3.4(b)). The position \mathbf{c}_k (relative to the origin O) of the apex of the cone is [24]

$$\mathbf{c}_k = \mathbf{r}_k + \omega_0^{-1} \mathbf{y}_k, \quad (3.15)$$

where $\omega_0 \neq 0$ and the chordal radius of the circle is $|\omega_0|^{-1}$. The velocity of \mathbf{c}_k along solutions of (3.14) is $\dot{\mathbf{c}}_k \triangleq \frac{r'}{dt} \mathbf{c}_k = (1 - \omega_0^{-1} \nu_k) \mathbf{x}_k$. We call \mathbf{c}_k the *center* of the circular formation.

Lemma 3. [24, Proposition 2] *The (constant) control $\nu_k = \omega_0$ steers particle k in model (3.14) around a circle such that the center \mathbf{c}_k is fixed, i.e., $\dot{\mathbf{c}}_k = \mathbf{0}$, where \mathbf{c}_k is defined in (3.15). A circular formation of N particles is characterized by the condition $\mathbf{c}_k = \mathbf{c}_j$ for all pairs $j, k \in \{1, \dots, N\}$.*

3.2.3 Particle Dynamics in a Time-Varying Flowfield

We now study the case of N particles traveling on the surface of a rotating sphere in a time-varying flowfield. The velocity of the flow at the position \mathbf{r}_k is represented by $\mathbf{f}_k(t) = \mathbf{f}(\mathbf{r}_k, t)$, which can be decomposed into vector components in frame \mathcal{C}_k :

$$\mathbf{f}_k(t) = p_k(t) \mathbf{x}_k + t_k(t) \mathbf{y}_k, \quad (3.16)$$

where $p_k(t) = \mathbf{f}_k(t) \cdot \mathbf{x}_k$ and $t_k(t) = \mathbf{f}_k(t) \cdot \mathbf{y}_k$. (Due to the assumption that \mathbf{z}_k is perpendicular to the flow, the dot product $\mathbf{f}_k(t) \cdot \mathbf{z}_k$ is identically zero.) The assumptions A1–A3 listed in Section 3.1.2 still apply in the spherical model. Adding (3.16) to the time derivative of the position of the particle model in (3.14) we obtain

$$\dot{\mathbf{r}}_k = (1 + p_k(t)) \mathbf{x}_k + t_k(t) \mathbf{y}_k.$$

Since $\dot{\mathbf{z}}_k$ is parallel to $\dot{\mathbf{r}}_k$, i.e., $\dot{\mathbf{z}}_k = \rho_0^{-1} \dot{\mathbf{r}}_k$, and the dynamics evolve on $SO(3)$, the remaining equations of motion can be found by computing the skew-symmetric matrix

$$\hat{\boldsymbol{\eta}}_k = \begin{bmatrix} 0 & -\nu_k & \rho_0^{-1} [1 + p_k(t)] \\ \nu_k & 0 & \rho_0^{-1} t_k(t) \\ -\rho_0^{-1} [1 + p_k(t)] & -\rho_0^{-1} t_k(t) & 0 \end{bmatrix},$$

such that $\dot{R}_k = R_k \hat{\boldsymbol{\eta}}_k$, where $R_k \triangleq [\mathbf{x}_k \ \mathbf{y}_k \ \mathbf{z}_k] \in SO(3)$. The equations of motion are

$$\begin{aligned} \dot{\mathbf{r}}_k &= [1 + p_k(t)] \mathbf{x}_k + t_k(t) \mathbf{y}_k \\ \dot{\mathbf{x}}_k &= \nu_k \mathbf{y}_k - \rho_0^{-1} [1 + p_k(t)] \mathbf{z}_k \\ \dot{\mathbf{y}}_k &= -\nu_k \mathbf{x}_k - \rho_0^{-1} t_k(t) \mathbf{z}_k \\ \dot{\mathbf{z}}_k &= \rho_0^{-1} [1 + p_k(t)] \mathbf{x}_k + \rho_0^{-1} t_k(t) \mathbf{y}_k, \end{aligned} \tag{3.17}$$

where $p_k(t) = \mathbf{f}_k(t) \cdot \mathbf{x}_k$, $t_k(t) = \mathbf{f}_k(t) \cdot \mathbf{y}_k$, and $\nu_k = u_k - 2\omega_1 z_{k3}$.

In order to find a control law to stabilize a formation in a time-varying flow, we transform the dynamics (3.17) using frame $\mathcal{D}_k = (k, \tilde{\mathbf{x}}_k, \tilde{\mathbf{y}}_k, \tilde{\mathbf{z}}_k)$, shown in Figure 3.3(e). The motion of a particle in a flowfield that is tangent to the sphere can be determined by summing the motion of the particle relative to the flow and the motion of the flow relative to the sphere. Consequently, we choose $\tilde{\mathbf{x}}_k$ to be parallel to $\dot{\mathbf{r}}_k$. The speed of particle k relative to \mathcal{I}' is denoted $s_k(t)$. The dynamics expressed in frame \mathcal{D}_k are

$$\begin{aligned} \dot{\mathbf{r}}_k &= s_k(t) \tilde{\mathbf{x}}_k \\ \dot{\tilde{\mathbf{x}}}_k &= \tilde{\nu}_k \tilde{\mathbf{y}}_k - \rho_0^{-1} s_k(t) \tilde{\mathbf{z}}_k \\ \dot{\tilde{\mathbf{y}}}_k &= -\tilde{\nu}_k \tilde{\mathbf{x}}_k \\ \dot{\tilde{\mathbf{z}}}_k &= \rho_0^{-1} s_k(t) \tilde{\mathbf{x}}_k, \end{aligned} \tag{3.18}$$

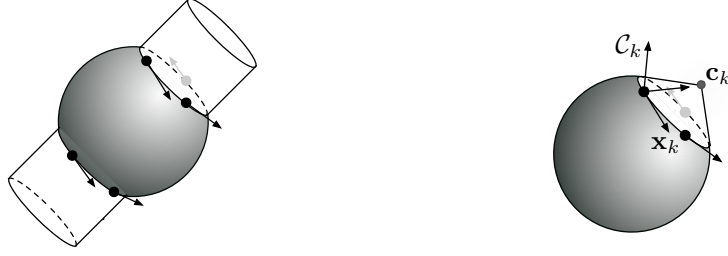


Figure 3.4: (a) Circular formation on the sphere. (b) The intersection of a right circular cone and the sphere results in a circular trajectory. The apex of the cone is called the *center* of the trajectory.

where \tilde{v}_k is the control input. Note, the dynamics in (3.18) still evolve on $SO(3)$.

In \mathcal{D}_k , the *center* of the circular formation is

$$\tilde{\mathbf{c}}_k = \mathbf{r}_k + \omega_0^{-1} \tilde{\mathbf{y}}_k. \quad (3.19)$$

The velocity of $\tilde{\mathbf{c}}_k$ along solutions of (3.18) is $\dot{\tilde{\mathbf{c}}}_k = (s_k(t) - \omega_0^{-1} \tilde{v}_k) \tilde{\mathbf{x}}_k$. The following extends Lemma 3 to motion on a rotating sphere in a time-varying flowfield.

Lemma 4. *Let $\mathbf{f}_k(t) = \mathbf{f}(\mathbf{r}_k, t)$ be a three-dimensional, time-varying flowfield that satisfies assumptions A1–A3 in Section 3.1.2. The control $\tilde{v}_k = \omega_0 s_k(t)$ steers particle k in model (3.18) around a circle such that the center $\tilde{\mathbf{c}}_k$ is fixed, i.e., $\dot{\tilde{\mathbf{c}}}_k = 0$, where $\tilde{\mathbf{c}}_k$ is defined in (3.19). A circular formation of N particles is characterized by the condition $\tilde{\mathbf{c}}_k = \tilde{\mathbf{c}}_j$ for all pairs $j, k \in \{1, \dots, N\}$.*

We now derive the relationship between frames \mathcal{C}_k and \mathcal{D}_k . This relationship is important because we design \tilde{v}_k using (3.18) and the platform dynamics are presumed to obey (3.14). Since $\tilde{\mathbf{z}}_k = \mathbf{z}_k$, we use (3.17) and (3.18) to write the following identity,

$$\tilde{\mathbf{x}}_k = s_k(t)^{-1} [(1 + p_k(t)) \mathbf{x}_k + t_k(t) \mathbf{y}_k]. \quad (3.20)$$

We find a relationship between $\tilde{\nu}_k$ and ν_k by taking the time derivative on each side of (3.20) and comparing terms to obtain

$$\nu_k = \tilde{\nu}_k + \frac{\dot{s}_k(t)t_k - s_k(t)\dot{t}_k(t)}{s_k(t)(1 + p_k(t))}.$$

By following the procedure for Case (i) in Appendix A, this equation is non-singular and, therefore, it is possible to compute ν_k from $\tilde{\nu}_k$.

From (3.20), the value of the inertial speed $s_k(t)$ is

$$s_k(t) = \|s_k(t)\tilde{\mathbf{x}}_k\| = \sqrt{(1 + p_k(t))^2 + t_k^2(t)} > 0,$$

where $p_k(t)$ and $t_k(t)$ are the components of $\mathbf{f}_k(t)$ in frame \mathcal{C}_k . However, in order to integrate (3.18) we must express $s_k(t)$ in terms of the components of $\mathbf{f}_k(t)$ in frame \mathcal{D}_k . Such an expression is provided by Theorem 4.

Chapter 4

Design of Decentralized Motion Coordination Algorithms

For both the three-dimensional and spherical models described in Chapter 3 we design Lyapunov-based decentralized control laws that stabilize particle formations. We stabilize parallel formations in the three-dimensional model in Section 4.1 and helical formations in the three-dimensional model in Section 4.2. In the spherical model we stabilize circular formations in Section 4.3.

4.1 Stabilization of Parallel Formations in a Three-Dimensional Flowfield

In this section, we derive decentralized control laws that stabilize parallel formations in a three-dimensional, time-varying flowfield, following the flow-free approach provided in [14] and [30]. A parallel formation is a steady motion in which all of the particles travel in straight, parallel lines with arbitrary separation. We provide a control law to stabilize parallel formations in an arbitrary direction and a control law that prescribes the direction. We use a graph G to represent the communication topology between the particles, which is connected, undirected, and time-invariant.

4.1.1 Parallel Formation with Arbitrary Direction

Let $G = (\mathcal{N}, E)$, where $\mathcal{N} = \{1, \dots, N\}$, denote a time-invariant, undirected, and connected graph with edge set E and graph Laplacian L [7] (see Section 2.3). Using the matrix $\mathcal{L} \triangleq L \otimes I_3$, where \otimes denotes the Kronecker product, we define the quadratic potential¹

$$S(\tilde{\mathbf{x}}) \triangleq \frac{1}{2} \tilde{\mathbf{x}}^T \mathcal{L} \tilde{\mathbf{x}} = \frac{1}{2} \sum_{(j,k) \in E} \|\tilde{\mathbf{x}}_j - \tilde{\mathbf{x}}_k\|^2, \quad (4.1)$$

where $\tilde{\mathbf{x}} \triangleq [\tilde{\mathbf{x}}_1^T \cdots \tilde{\mathbf{x}}_N^T]^T$ and the summation is over all of the edges in G . The potential S is minimized by the set of parallel formations in accordance with Lemma 2.

Using (3.4) we find the time derivative of S along solutions of (3.3) to be

$$\dot{S} = \sum_{j=1}^N \dot{\tilde{\mathbf{x}}}_j \cdot \mathcal{L}_j \tilde{\mathbf{x}} = \sum_{j=1}^N \left(\tilde{R}_j \tilde{\mathbf{u}}_j \times \tilde{\mathbf{x}}_j \right) \cdot \mathcal{L}_j \tilde{\mathbf{x}},$$

where \mathcal{L}_k denotes three consecutive rows of \mathcal{L} starting with row $3k - 2$, $k \in \mathcal{N}$.

Choosing the control law

$$\tilde{\mathbf{u}}_k = -K_0 \tilde{R}_k^T (\tilde{\mathbf{x}}_k \times \mathcal{L}_k \tilde{\mathbf{x}}), \quad K_0 > 0, \quad (4.2)$$

ensures that S is nonincreasing, since ²

$$\dot{S} = -K_0 \sum_{j=1}^N (\tilde{\mathbf{x}}_j \times \mathcal{L}_j \tilde{\mathbf{x}} \times \tilde{\mathbf{x}}_j) \cdot \mathcal{L}_j \tilde{\mathbf{x}} = -K_0 \sum_{j=1}^N \|\tilde{\mathbf{x}}_j \times \mathcal{L}_j \tilde{\mathbf{x}}\|^2 \leq 0. \quad (4.3)$$

The following extends [30, Theorem 1] to motion in a spatially and/or temporally variable flowfield.

¹We drop the subscript to denote the matrix collection of N elements, e.g., $\mathbf{x} \triangleq [\mathbf{x}_1^T \cdots \mathbf{x}_N^T]^T$, which is a $3N \times 1$ matrix.

²Proof is given in Appendix E.

Theorem 5. *Let $\mathbf{f}_k(t) = \mathbf{f}(\mathbf{r}_k, t)$ be a three-dimensional, time-varying flowfield that satisfies assumptions A1–A3 in Section 3.1.2. Assume the particle communication topology is defined by a time-invariant, undirected, and connected graph G , with graph Laplacian L . All solutions of the closed-loop model (3.3), where the speed $s_k(t)$ is given by (3.8) and the control $\tilde{\mathbf{u}}_k$ by (4.2), converge to the set $\{\dot{S} = 0\}$, where S is defined in (4.1). The set of parallel formations is uniformly asymptotically stable and the direction of motion is determined by the initial conditions. If G is the complete graph, then every other positive limit set is unstable.*

Proof. The closed-loop dynamics $\dot{\tilde{\mathbf{x}}}_k = \tilde{R}_k \tilde{\mathbf{u}}_k \times \tilde{\mathbf{x}}_k$ with $\tilde{\mathbf{u}}_k$ given by (4.2) are autonomous and independent of the flowfield and, therefore, we use Theorems 1 and 2 in Chapter 2 to prove our results. (We do need $\mathbf{f}_k(t)$ to at least satisfy assumptions A1 and A2 in Section 3.1.2 in order for the model (3.3) to be well-defined.) The proof follows the proof of [30, Theorem 1]. Since each $\tilde{\mathbf{x}}_k$ has unit length, the dynamics evolve on a compact space isomorphic to N copies of the two-sphere S^2 . The potential S is radially unbounded, positive-definite in the reduced space of relative velocities, and its time derivative satisfies $\dot{S} \leq 0$. The potential S is zero if and only if $\tilde{\mathbf{x}}_j = \tilde{\mathbf{x}}_k \forall j, k \in \mathcal{N}$. By the invariance principle, all solutions converge to the largest invariant set in $\{\dot{S} = 0\}$, for which $\tilde{\mathbf{x}}_k \times \mathcal{L}_k \tilde{\mathbf{x}} = 0, k \in \mathcal{N}$. When $\mathcal{L}_k \tilde{\mathbf{x}} = 0 \forall k$, the potential S is minimized, forming the set of parallel formations $\tilde{\mathbf{x}}_j = \tilde{\mathbf{x}}_k \forall j, k \in \mathcal{N}$. Since this set corresponds to the global minimum of S , it is asymptotically stable, uniformly in time. In the case of all-to-all communication, solutions in the set $\{\dot{S} = 0\}$ also consist of balanced formations and anti-parallel

formations [30]. The set of balanced formations, for which the average over all $\tilde{\mathbf{x}}_k$ is zero, maximize the potential S and are unstable [30]. The set of anti-parallel formations, for which $\tilde{\mathbf{x}}_k = \pm\tilde{\mathbf{x}}_j$ for all pairs k and j , are saddle points, since all anti-parallel formations contain two groups moving in opposite directions and a small variation of any $\tilde{\mathbf{x}}_k$ in the smaller (resp. larger) group leads to a decrease (resp. increase) in the value of S [30]. \square

Theorem 5 provides a decentralized algorithm to stabilize a parallel formation in a three-dimensional flowfield using control (4.2). The results are simulated in Figure 4.1. The direction of motion of the formation is determined by the initial conditions. The flowfield is a three-dimensional adaptation of a Rankine vortex [21], with maximum flow speed occurring on a set of radii that increases with height. The vortex center translates horizontally and therefore represents a time-varying flowfield.

4.1.2 Parallel Formation in a Prescribed Direction

Control (4.2) stabilizes parallel formations that travel in an arbitrary direction. Next we provide a control algorithm that stabilizes parallel formations travelling in a prescribed direction. For this, we introduce a virtual particle (indexed by $k = 0$), that travels in the prescribed direction $\boldsymbol{\omega}_0$. The dynamics of particle 0 are given by (3.3) with $\tilde{\mathbf{u}}_0 = 0$ and $\tilde{\mathbf{x}}_0(t) = \tilde{\mathbf{x}}_0(0) = \boldsymbol{\omega}_0/\|\boldsymbol{\omega}_0\|$.

Let $G = (\mathcal{N}, E)$, where $\mathcal{N} = \{1, \dots, N\}$, denote a time-invariant, undirected, and connected graph with edge set E and graph Laplacian L . Also, let $G_0 =$

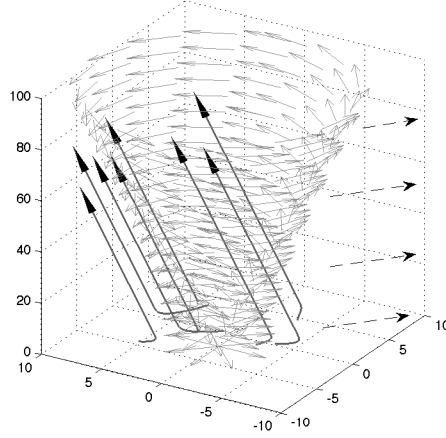


Figure 4.1: Stabilization of particle model (3.3) with $N = 8$ to parallel motion in an arbitrary direction in a time-varying flowfield using control (4.2). The dashed arrows represent the translational movement of the flow.

(\mathcal{N}_0, E_0) , where $\mathcal{N}_0 = \{0, 1, \dots, N\}$, denote a time-invariant and directed graph rooted to node 0. The edge set $E_0 \subset E$ includes at least one link from particle 0 to a particle $k \in \mathcal{N}$. L_0 is the Laplacian matrix of G_0 . We define the augmented potential

$$S_0 = \frac{1}{2} \sum_{(j,k) \in E_0} \|\tilde{\mathbf{x}}_k - \tilde{\mathbf{x}}_j\|^2 = \frac{1}{2} \tilde{\mathbf{x}}^T \mathcal{L} \tilde{\mathbf{x}} + \frac{1}{2} \sum_{j=1}^N a_{j0} \|\tilde{\mathbf{x}}_j - \tilde{\mathbf{x}}_0\|^2, \quad (4.4)$$

where $a_{j0} = 1$ if there is information flow from particle 0 to particle $j \in \mathcal{N}$, and $a_{j0} = 0$ otherwise. Using (3.4), the time derivative of S_0 is

$$\begin{aligned} \dot{S}_0 &= \sum_{j=1}^N \left[\tilde{\mathbf{x}}_j \cdot \mathcal{L}_j \tilde{\mathbf{x}} + a_{j0} \left(\tilde{\mathbf{x}}_j - \frac{\boldsymbol{\omega}_0}{\|\boldsymbol{\omega}_0\|} \right) \cdot \dot{\tilde{\mathbf{x}}}_j \right] \\ &= - \sum_{j=1}^N \left[\tilde{R}_j \tilde{\mathbf{u}}_j \times \tilde{\mathbf{x}}_j \right] \cdot \left[\mathcal{L}_j \tilde{\mathbf{x}} - a_{j0} \left(\tilde{\mathbf{x}}_j - \frac{\boldsymbol{\omega}_0}{\|\boldsymbol{\omega}_0\|} \right) \right]. \end{aligned}$$

Choosing

$$\tilde{\mathbf{u}}_k = K_0 \tilde{R}_k^T \left[\tilde{\mathbf{x}}_k \times \left(\mathcal{L}_k \tilde{\mathbf{x}} - a_{k0} \left(\tilde{\mathbf{x}}_k - \frac{\boldsymbol{\omega}_0}{\|\boldsymbol{\omega}_0\|} \right) \right) \right], \quad K_0 > 0, \quad (4.5)$$

yields

$$\dot{S}_0 = -K_0 \sum_{j=1}^N \left\| \tilde{\mathbf{x}}_j \times \left(\mathcal{L}_j \tilde{\mathbf{x}} - a_{j0} \left(\tilde{\mathbf{x}}_j - \frac{\boldsymbol{\omega}_0}{\|\boldsymbol{\omega}_0\|} \right) \right) \right\|^2 \leq 0,$$

which ensures that S_0 is non-increasing.

Corollary 1. *Let $\mathbf{f}_k(t) = \mathbf{f}(\mathbf{r}_k, t)$ be a three-dimensional, time-varying flowfield that satisfies assumptions A1–A3 in Section 3.1.2. Assume the particle communication topology is defined by a time-invariant, undirected, and connected graph G , with graph Laplacian L . Let $G_0 \subset G$ be a time-invariant and directed graph rooted to node 0, with graph Laplacian L_0 . All solutions of the closed-loop model (3.3), where the speed $s_k(t)$ is given by (3.8) and the control $\tilde{\mathbf{u}}_k$ by (4.5), converge to the set $\{\dot{S}_0 = 0\}$, where S_0 is defined in (4.4). The set of parallel formations is uniformly asymptotically stable and the direction of motion is determined by $\boldsymbol{\omega}_0$. If G_0 is the complete graph, then every other positive limit set is unstable.*

Figure 4.2 shows a parallel stabilization in the vertical direction, prescribed by $\boldsymbol{\omega}_0 = [0 \ 0 \ 1]^T$. We simulate model (3.3) using control (4.5) in a three-dimensional adaptation of a Rankine vortex flowfield that translates horizontally.

4.2 Stabilization of Helical Formations in a Three-Dimensional Flowfield

We seek to design a decentralized control law to stabilize a helical formation in a time-varying flowfield. A helical formation is a steady three-dimensional motion in which all of all the particles converge to circular helices with the same axis

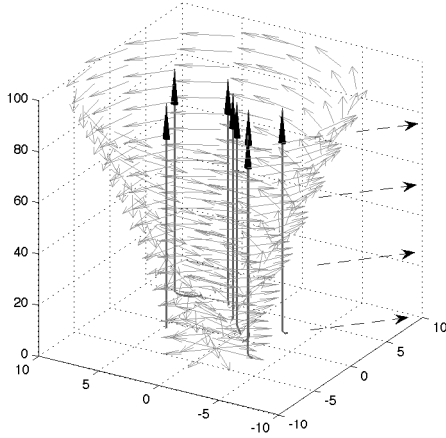


Figure 4.2: Stabilization of model (3.3) with $N = 8$ particles to parallel motion in the desired direction $\boldsymbol{\omega}_0 = [0 \ 0 \ 1]^T$ in a time-varying flowfield using control (4.5).

of rotation, radius, and pitch. We provide control laws to stabilize (A) helical formations with arbitrary center and arbitrary or prescribed pitch and (B) prescribed center and prescribed pitch.

4.2.1 Helical Formation with Arbitrary Pitch

Let $G = (\mathcal{N}, E)$, where $\mathcal{N} = \{1, \dots, N\}$, denote a time-invariant, undirected, and connected graph, with graph Laplacian L and $\mathcal{L} \triangleq L \otimes I_3$ (see Section 2.3).

The quadratic potential

$$Q(\tilde{\mathbf{v}}^a) = \frac{1}{2} (\tilde{\mathbf{v}}^a)^T \mathcal{L} \tilde{\mathbf{v}}^a = \frac{1}{2} \sum_{(j,k) \in E} \|\tilde{\mathbf{v}}_j^a - \tilde{\mathbf{v}}_k^a\|^2, \quad (4.6)$$

where $\tilde{\mathbf{v}}_k^a$ is defined in (3.6), is minimized by the set of helical formations in accordance with Lemma 1. Recall \mathcal{L}_k , $k \in 1, \dots, N$, denotes three consecutive rows of \mathcal{L}

starting with row $3k - 2$. Along solutions of (3.3),

$$\dot{Q} = \sum_{j=1}^N \mathcal{L}_j \tilde{\mathbf{v}}^a \cdot (\dot{\tilde{\mathbf{x}}}_j + \dot{\mathbf{r}}_j \times \boldsymbol{\omega}_0) = \sum_{j=1}^N \mathcal{L}_j \tilde{\mathbf{v}}^a \cdot \left[\tilde{\mathbf{x}}_j \times (s_j(t)\boldsymbol{\omega}_0 - \tilde{R}_j \tilde{\mathbf{u}}_j) \right].$$

Choosing

$$\tilde{\mathbf{u}}_k = K_0 \tilde{R}_k^T [s_k(t)\boldsymbol{\omega}_0 + \mathcal{L}_k \tilde{\mathbf{v}}^a \times \tilde{\mathbf{x}}_k], \quad K_0 > 0, \quad (4.7)$$

results in

$$\dot{Q} = -K_0 \sum_{j=1}^N \mathcal{L}_j \tilde{\mathbf{v}}^a \cdot (\tilde{\mathbf{x}}_j \times \mathcal{L}_j \tilde{\mathbf{v}}^a \times \tilde{\mathbf{x}}_j) = - \sum_{j=1}^N \|\tilde{\mathbf{x}}_j \times \mathcal{L}_j \tilde{\mathbf{v}}^a\|^2 \leq 0.$$

The following result extends [30, Theorem 2] to motion in a spatially and/or temporally variable flowfield.

Theorem 6. *Let $\mathbf{f}_k(t) = \mathbf{f}(\mathbf{r}_k, t)$ be a three-dimensional, time-varying flowfield that satisfies assumptions A1–A3 in Section 3.1.2. Assume the particle communication topology is defined by an undirected, connected, and time-invariant graph G , with graph Laplacian L . All solutions of the closed-loop model (3.3), where the speed $s_k(t)$ is given by (3.8) and the control $\tilde{\mathbf{u}}_k$ by (4.7), converge to the set $\{\dot{Q} = 0\}$, where Q is defined in (4.6). The set of helical formations with axis of rotation parallel to $\boldsymbol{\omega}_0$, radius $\|\boldsymbol{\omega}_0\|^{-1}$, and arbitrary pitch is uniformly asymptotically stable and the formation pitch and center are determined by the initial conditions. If G is the complete graph, then every other positive limit set is unstable.*

Proof. The closed-loop dynamics (3.3) with $\tilde{\mathbf{u}}_k$ given in (4.7) depend on the time-varying speed $s_k(t)$. Therefore, the proof follows from application of an invariance-like theorem for non-autonomous systems [15, Theorem 8.4], stated in Theorem 3

in Chapter 2. Q is radially unbounded and positive definite in the reduced space of $\tilde{\mathbf{v}}_k^a - \tilde{\mathbf{v}}_j^a \forall j, k \in \mathcal{N}$. The time derivative of Q satisfies $\dot{Q} \leq 0$ and neither Q nor \dot{Q} depend explicitly on time. The potential Q is zero if and only if $\tilde{\mathbf{v}}_j^a = \tilde{\mathbf{v}}_k^a \forall k, j \in \mathcal{N}$. By Theorem 3 all solutions of the closed-loop model converge to the set $\{\dot{Q} = 0\}$, in which $\tilde{\mathbf{x}}_k \times \mathcal{L}_k \tilde{\mathbf{v}}^a = 0 \forall k$. The remainder of the proof follows the proof of [30, Theorem 2]. We consider three cases. (i) When $\mathcal{L}_k \tilde{\mathbf{v}}^a = 0 \forall k \in \mathcal{N}$ (which corresponds to $\dot{\tilde{\mathbf{x}}}_k = s_k(t) \boldsymbol{\omega}_0 \times \tilde{\mathbf{x}}_k \neq 0 \forall k$ in steady-state), the potential Q is minimized, forming the set of helical formations $\tilde{\mathbf{v}}_j^a = \tilde{\mathbf{v}}_k^a \forall k, j \in \mathcal{N}$. Since this set corresponds to the global minimum of Q , it is asymptotically stable, uniformly in time. (ii) In the case of all-to-all communication, $\boldsymbol{\omega}_0$ is parallel to $\tilde{\mathbf{x}}_k \forall k$ when, in steady-state, $s_k(t) \boldsymbol{\omega}_0 \times \tilde{\mathbf{x}}_k = 0 \forall k$. Solutions of the closed-loop model converge to the set in which $\boldsymbol{\omega}_0 \times \mathcal{L}_k \tilde{\mathbf{v}}^a = 0 \forall k$, which requires \mathbf{r}_k be parallel to $\boldsymbol{\omega}_0$. When $\tilde{\mathbf{x}}_k$ and \mathbf{r}_k are parallel to $\boldsymbol{\omega}_0 \forall k \in \mathcal{N}$, the set corresponds to parallel formations, which are helical formations with infinite pitch, and the stability of this result is the same as in Theorem 5. (iii) We are still left with the situation when $s_k(t) \boldsymbol{\omega}_0 \times \tilde{\mathbf{x}}_k \neq 0$ for $k \in G_1$ and $s_k(t) \boldsymbol{\omega}_0 \times \tilde{\mathbf{x}}_k \neq 0$ for $k \in G_2$, where G_1 and G_2 are two disjoint groups of particles such that $|G_1| = M$ and $|G_2| = N - M$ [30]. We have $\mathcal{L}_k \tilde{\mathbf{v}}^a = 0, k \in G_1$ and $\boldsymbol{\omega}_0 \times \mathcal{L}_k \tilde{\mathbf{v}}^a = 0, j \in G_2$. Following [30, Theorem 2], this set does not correspond to a minimum of Q and is unstable. \square

Theorem 6 provides a method to stabilize helical formations in a three-dimensional flowfield. Note, Theorem 6 guarantees positive invariance of the set of helical formations when $\mathbf{f}_k(t) = \mathbf{f}_k(0)$. Figure 4.3(a) shows flow-induced instability of the

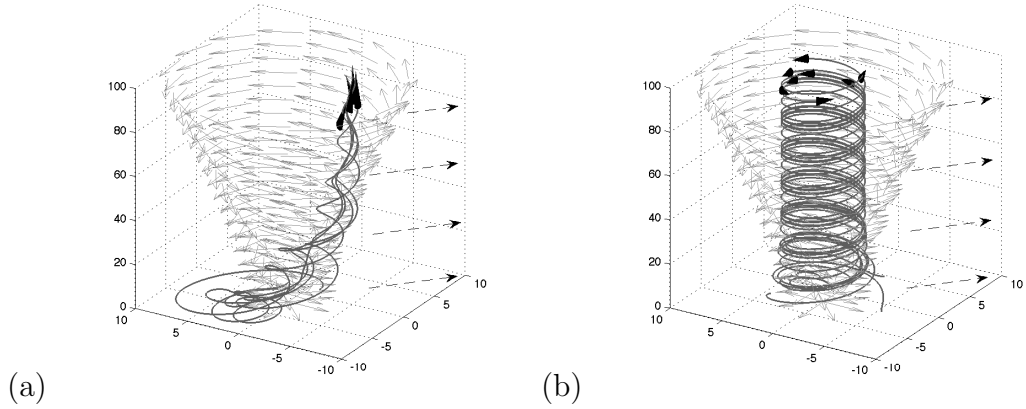


Figure 4.3: Stabilization of helical motion in a three-dimensional, time-varying flowfield in model (3.3). Parameter values are $N = 8$, $K_0 = 0.24$, and $\boldsymbol{\omega}_0 = [0 \ 0 \ 1]^T$. (a) The control used in [31] is implemented in the dynamics with flow using $N = 5$ particles. The particles do not converge to helical formation. (b) Control (4.7) stabilizes all particles to helical formation. The dashed arrows represent the translational movement of the flow.

helical control designed using the flow-free model (3.1) [31]. Figure 4.3(b) depicts a helical formation stabilized using control (4.7) in the translating Rankine vortex, using model (3.3).

4.2.2 Helical Formation with a Prescribed Pitch and Center

The pitch and center of a helical formation stabilized by control (4.7) are determined by the initial conditions. To isolate helical formations with a prescribed pitch and prescribed center we use the following method adapted from [30]. We introduce a virtual particle (indexed by $k = 0$) with dynamics given by (3.3) with $\tilde{\mathbf{u}}_0 = s_k(t)\tilde{R}_k\boldsymbol{\omega}_0$, so that $\tilde{\mathbf{v}}_0^a(t) = \tilde{\mathbf{v}}_0^a(0) \forall t$. The *twist* (see Section 2.1.4) of particle 0, $\tilde{\boldsymbol{\xi}}_0^a = [(\tilde{\mathbf{v}}_0^a)^T, \boldsymbol{\omega}_0^T]^T$, is constant and its corresponding pitch is $\tilde{\mathbf{v}}_0^a \cdot \boldsymbol{\omega}_0 / \|\boldsymbol{\omega}_0\|^2$ [20, 30].

Let $G = (\mathcal{N}, E)$, where $\mathcal{N} = \{1, \dots, N\}$, denote a time-invariant, undirected, and connected graph with edge set E and graph Laplacian L [7]. Also, let $G_0 = (\mathcal{N}_0, E_0)$, where $\mathcal{N}_0 = \{0, 1, \dots, N\}$, denote a time-invariant and directed graph rooted to node 0. The edge set $E_0 \subset E$ includes at least one link from particle 0 to a particle $k \in \mathcal{N}$. L_0 is the Laplacian matrix of G_0 .

We first isolate helical formations with a prescribed pitch. To do so, we define the pitch parameter $\alpha_0 \in [0, 1)$. Note that a pitch of $\alpha_0 = 0$ results in a circular formation and, as α_0 approaches 1, the helical formation becomes increasingly parallel. The potential [30]

$$Q_1 = \frac{1}{2} \sum_{j=1}^N a_{j0} \beta_j^2, \quad (4.8)$$

where $\beta_j = \tilde{\mathbf{v}}_j^a \cdot \boldsymbol{\omega}_0 / \|\boldsymbol{\omega}_0\| - \alpha_0$ and $\tilde{\mathbf{v}}_j^a$ is defined in (3.6), is minimum when the pitch of all particles $j \in \mathcal{N}$ is equal to α_0 . The constant $a_{j0} = 1$ if there is information flow from particle 0 to particle $j \in \mathcal{N}$, and $a_{j0} = 0$ otherwise.

We find a control law that stabilizes a helical formation with a prescribed pitch by defining the following augmented potential, determined by the sum of (4.6) and (4.8):

$$Q_0 = \frac{1}{2} (\tilde{\mathbf{v}}^a)^T \mathcal{L} \tilde{\mathbf{v}}^a + \frac{1}{2} \sum_{j=1}^N a_{j0} \beta_j^2, \quad (4.9)$$

The time derivative of Q_0 is

$$\dot{Q}_0 = \sum_{j=1}^N \left[\mathcal{L}_j \tilde{\mathbf{v}}^a + a_{j0} \beta_j \frac{\boldsymbol{\omega}_0}{\|\boldsymbol{\omega}_0\|} \right] \cdot \left[(\tilde{R}_j \tilde{\mathbf{u}}_j - s_j \boldsymbol{\omega}_0) \times \tilde{\mathbf{x}}_j \right].$$

We ensure $\dot{Q}_0 \leq 0$ by choosing the control

$$\tilde{\mathbf{u}}_k = K_0 \tilde{R}_k^T \left[s_k(t) \boldsymbol{\omega}_0 + \left(\mathcal{L}_k \tilde{\mathbf{v}}^a + a_{k0} \beta_k \frac{\boldsymbol{\omega}_0}{\|\boldsymbol{\omega}_0\|} \right) \times \tilde{\mathbf{x}}_k \right], \quad K_0 > 0. \quad (4.10)$$

Corollary 2. *Let $\mathbf{f}_k(t) = \mathbf{f}(\mathbf{r}_k, t)$ be a three-dimensional, time-varying flowfield that satisfies assumptions A1–A3 in Section 3.1.2. Assume the particle communication topology is defined by a time-invariant, undirected, and connected graph G , with graph Laplacian L . Let $G_0 \subset G$ be a time-invariant and directed graph rooted to node 0, with graph Laplacian L_0 . All solutions of the closed-loop model (3.3), where the speed $s_k(t)$ is given by (3.8) and the control $\tilde{\mathbf{u}}_k$ by (4.10), converge to the set $\{\dot{Q}_0 = 0\}$, where Q_0 is defined in (4.9). The set of helical formations with pitch α_0 , axis of rotation parallel to $\boldsymbol{\omega}_0$ and radius $\|\boldsymbol{\omega}_0\|^{-1}$ is uniformly asymptotically stable and the formation center is determined by the initial conditions. If G is the complete graph, every other positive limit set is unstable.*

Corollary 2 provides an algorithm to isolate a set of helical formations with prescribed pitch α_0 . An interesting case is when we set $\alpha_0 = 0$, in which control (4.10) stabilizes a circular formation, as shown in Figure 4.4.

We now isolate helical formations with a prescribed pitch and center. The control law (4.7) uses the parameter $\boldsymbol{\omega}_0$, which prescribes a line parallel to the axis of rotation of the helical formation, but not the exact location of this axis. To prescribe the *center*, which is a point on the axis of the formation, we define the potential

$$Q_2 = \frac{1}{2} \sum_{j=1}^N a_{j0} \|\tilde{\mathbf{v}}_j^a - \tilde{\mathbf{v}}_0^a\|^2, \quad (4.11)$$

where $\tilde{\mathbf{v}}_j^a$ is defined in (3.6). Q_2 is minimum when $\tilde{\mathbf{v}}_k^a = \tilde{\mathbf{v}}_0^a \forall k \in \mathcal{N}$ and the center of the formation is a point on $\tilde{\mathbf{v}}_0^a$.

To find a control law that will stabilize a helical formation with a prescribed

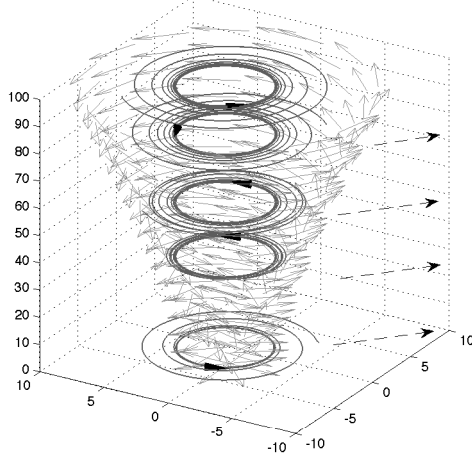


Figure 4.4: Stabilization of helical motion with prescribed pitch. Control (4.10) stabilizes all particles of model (3.3) to a formation with zero pitch ($\alpha_0 = 0$), which is a circular formation. Parameter values are $N = 5$, $K_0 = 0.3$, and $\boldsymbol{\omega}_0 = [0 \ 0 \ 1]^T$.

pitch and center, we define the following augmented potential, determined by the sum of (4.9) and (4.11):

$$\tilde{Q}_0 = \frac{1}{2} \tilde{\mathbf{v}}^a T \mathcal{L} \tilde{\mathbf{v}}^a + \frac{1}{2} \sum_{j=1}^N a_{j0} (\beta^2 + \|\tilde{\mathbf{v}}_j^a - \tilde{\mathbf{v}}_0^a\|^2), \quad (4.12)$$

where $\beta_j = \tilde{\mathbf{v}}_j^a \cdot \boldsymbol{\omega}_0 / \|\boldsymbol{\omega}_0\| - \alpha_0$ and $\alpha_0 \in [0, 1)$. The time derivative of Q_0 is

$$\dot{\tilde{Q}}_0 = \sum_{j=1}^N \left[\tilde{\mathcal{L}}_j \tilde{\mathbf{v}}^a + a_{j0} \left(\beta \frac{\boldsymbol{\omega}_0}{\|\boldsymbol{\omega}_0\|} + \tilde{\mathbf{v}}_j^a - \tilde{\mathbf{v}}_0^a \right) \right] \cdot \left[(\tilde{R}_j \tilde{\mathbf{u}}_j - s_j \boldsymbol{\omega}_0) \times \tilde{\mathbf{x}}_j \right].$$

The control

$$\tilde{\mathbf{u}}_k = K_0 \tilde{R}_k^T \left[s_k(t) \boldsymbol{\omega}_0 + \left(\tilde{\mathcal{L}}_k \tilde{\mathbf{v}}^a + a_{k0} \left(\beta \frac{\boldsymbol{\omega}_0}{\|\boldsymbol{\omega}_0\|} + \tilde{\mathbf{v}}_k^a - \tilde{\mathbf{v}}_0^a \right) \right) \times \tilde{\mathbf{x}}_k \right], \quad K_0 > 0, \quad (4.13)$$

yields

$$\dot{\tilde{Q}}_0 = -K_0 \sum_{j=1}^N \left\| \tilde{\mathbf{x}}_j \times \left[\tilde{\mathcal{L}}_j \tilde{\mathbf{v}}^a + a_{j0} \left(\beta \frac{\boldsymbol{\omega}_0}{\|\boldsymbol{\omega}_0\|} + \tilde{\mathbf{v}}_j^a - \tilde{\mathbf{v}}_0^a \right) \right] \right\|^2 \leq 0,$$

which ensures that \tilde{Q}_0 is non-increasing.

Corollary 3. *Let $\mathbf{f}_k(t) = \mathbf{f}(\mathbf{r}_k, t)$ be a three-dimensional, time-varying flowfield that satisfies assumptions A1–A3 in Section 3.1.2. Assume the particle communication topology is defined by a time-invariant, undirected, and connected graph G , with graph Laplacian L . Let $G_0 \subset G$ be a time-invariant and directed graph rooted to node 0, with graph Laplacian L_0 . All solutions of the closed-loop model (3.3), where the speed $s_k(t)$ is given by (3.8) and the control $\tilde{\mathbf{u}}_k$ by (4.13), converge to the set $\{\dot{\tilde{Q}}_0 = 0\}$, where \tilde{Q}_0 is defined in (4.12). The set of helical formations centered on $\tilde{\mathbf{v}}_0^a$, with pitch α_0 , and radius $\|\boldsymbol{\omega}_0\|^{-1}$ is uniformly asymptotically stable and the formation center is determined by the initial conditions. If G is the complete graph, every other positive limit set is unstable.*

We use control (4.13) to stabilize a helical formation in model 3.3 with a prescribed pitch and center that passes through the vertical axis in the xy-plane in a time-varying flowfield. This is shown in Figure 4.5.

4.3 Stabilization of Circular Formations on a Rotating Sphere with Flow

We seek to design a decentralized control law that stabilizes circular motion in a time-varying flowfield on a rotating sphere with a common radius, axis of rotation and direction of rotation [24]. In Section 4.3.1 we design a control law to stabilize a circular formation on a rotating sphere. In Section 4.3.2 we design a control law to stabilize a circular formation with arbitrary center in a time-varying flowfield on a rotating sphere and in Section 4.3.3 we prescribe the center of the formation.

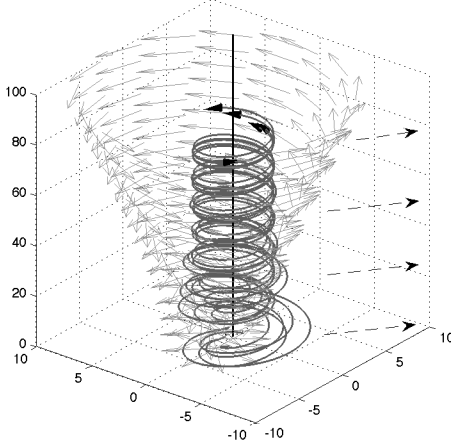


Figure 4.5: Stabilization of helical motion with prescribed center. Control (4.13) stabilizes all particles to helical formation with $\alpha_0 = 0.8$ and the center located at the origin of the xy -plane. Parameter values are $N = 6$, $K_0 = 0.1$, $\boldsymbol{\omega}_0 = [0 \ 0 \ 1]^T$, and $\tilde{\mathbf{v}}_0^a = [0 \ 0 \ 0]^T$.

4.3.1 Circular Formation on a Flow-Free Rotating Sphere

Let $G = (\mathcal{N}, E)$, where $\mathcal{N} = \{1, \dots, N\}$, denote a time-invariant, undirected, and connected graph, with graph Laplacian L and $\mathcal{L} \triangleq L \otimes I_3$ (see Section 2.3).

The quadratic potential [24]

$$V(\mathbf{r}, \mathbf{x}, \mathbf{y}, \mathbf{z}) \triangleq \frac{1}{2} \mathbf{c}^T \mathcal{L} \mathbf{c} = \frac{1}{2} \sum_{(j,k) \in E} \|\mathbf{c}_j - \mathbf{c}_k\|^2, \quad (4.14)$$

where $\mathcal{L} \triangleq L \otimes I_3$ and \mathbf{c}_k is defined in (3.15), is minimized by the set of circular formations on a sphere in accordance with Lemma 3. The time derivative of V along solutions of (3.14) is

$$\dot{V} = \sum_{j=1}^N \dot{\mathbf{c}}_j \cdot \mathcal{L}_j \mathbf{c} = \sum_{j=1}^N (1 - \omega_0^{-1} \nu_j) \mathbf{x}_j \cdot \mathcal{L}_j \mathbf{c},$$

where \mathcal{L}_k denotes three consecutive rows of \mathcal{L} starting with row $3k - 2$, $k \in \mathcal{N}$.

Choosing the control law

$$\nu_k = \omega_0(1 + K_0 \mathbf{x}_k \cdot \mathcal{L}_k \mathbf{c}), \quad K_0 > 0, \quad (4.15)$$

makes

$$\dot{V} = -K_0 \sum_{j=1}^N (\mathbf{x}_j \cdot \mathcal{L}_j \mathbf{c})^2 \leq 0,$$

which ensures that V is nonincreasing [24]. The following theorem extends [24, Theorem 4] to motion on a rotating sphere.

Theorem 7. *Assume the particle communication topology is defined by an undirected, connected, and time-invariant graph G , with graph Laplacian L . All solutions of the closed-loop model (3.14), where the control ν_k is given by (4.15), converge to the set $\{\dot{V} = 0\}$, where V is defined in (4.14). The set of circular formations with radius $|\omega_0|^{-1}$ and direction of rotation determined by the sign of ω_0 is uniformly asymptotically stable and all other positive limit sets are unstable.*

Proof. By the invariance principle, stated in Theorem 2 in Chapter 2, all solutions converge to the largest invariant set where $\mathbf{x}_k \cdot (\mathbf{c}_k - \mathbf{c}_j) = 0$ for all connected pairs j and k . This is a set of circular trajectories on the same or opposite sides of the sphere. The set of circular formations is asymptotically stable, because it corresponds to the global minimum of the potential. Suppose M particles are on one side of the sphere and $N - M$ particles are on the other side. By considering the change in V as a function of a variation of a particle in either group, we observe that (i) if N is even, then solutions with $M = N/2$ are local maxima; and (ii) for any

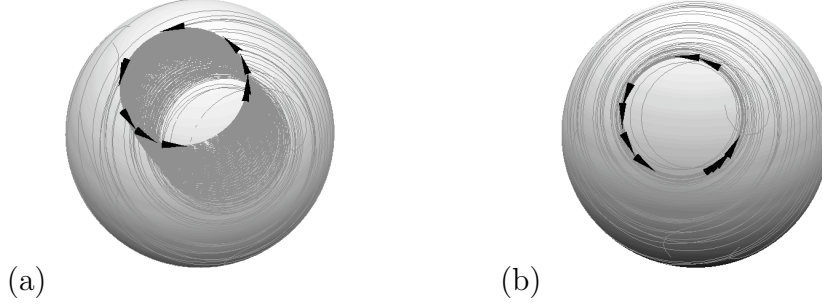


Figure 4.6: Stabilization of a circular formation on a rotating sphere using model (3.14). Parameters used are $N = 10$, $\rho_0 = 10$, $\omega_0 = 2$, $\omega_1 = 0.1$ and $K_0 = 0.01$. (a) Control (4.15) stabilizes a circular formation on a rotating sphere, but the formation is translated along the sphere due to the Coriolis effect. (b) Using control $u_k = \nu_k + 2\omega_1 z_{k3}$, where ν_k is given by (4.15), cancels the Coriolis effect and stabilizes a circular formation with a fixed center.

$N > 2$, solutions with $N > M > 0$ are saddles. Therefore, all solutions consisting of colocated circular trajectories on opposite sides of the sphere are unstable. \square

Simulating model (3.14) with control ν_k given by (4.15) stabilizes a circular formation on the rotating sphere, but the center is not fixed due to the Coriolis effect (see Figure 4.6 (a)). However, by using (3.13) to compute $u_k = \nu_k + 2\omega_1 z_{k3}$ we cancel the Coriolis effect and stabilize a circular formation with a fixed center (see Figure 4.6 (b)).

Next we incorporate a time-varying flow to the rotating spherical model.

4.3.2 Circular Formation with Arbitrary Center

We work in the frame \mathcal{D}_k to find a control law that stabilizes a circular formation in a time-varying flow on a rotating sphere. Again, let $G = (\mathcal{N}, E)$ denote a time-invariant and undirected graph with graph Laplacian L . The quadratic po-

tential

$$\tilde{V}(\mathbf{r}, \tilde{\mathbf{x}}, \tilde{\mathbf{y}}, \tilde{\mathbf{z}}) \triangleq \frac{1}{2} \tilde{\mathbf{c}}^T \mathcal{L} \tilde{\mathbf{c}} = \frac{1}{2} \sum_{(j,k) \in E}^N \|\tilde{\mathbf{c}}_j - \tilde{\mathbf{c}}_k\|^2, \quad (4.16)$$

where $\mathcal{L} \triangleq L \otimes I_3$ and $\tilde{\mathbf{c}}_k$ is defined in (3.19), is minimized by the set of circular formations on the sphere in accordance with Lemma 4. The time derivative of \tilde{V} along solutions of (3.18) is

$$\dot{\tilde{V}} = \sum_{j=1}^N \dot{\tilde{\mathbf{c}}}_j \cdot \mathcal{L}_j \tilde{\mathbf{c}} = \sum_{j=1}^N (s_j(t) - \frac{1}{\omega_0} \tilde{\nu}_j) \tilde{\mathbf{x}}_j \cdot \mathcal{L}_j \tilde{\mathbf{c}}.$$

Choosing the control law

$$\tilde{\nu}_k = \omega_0 (s_k(t) + K_0 \tilde{\mathbf{x}}_k \cdot \mathcal{L}_k \tilde{\mathbf{c}}), \quad K_0 > 0, \quad (4.17)$$

makes

$$\dot{\tilde{V}} = -K_0 \sum_{j=1}^N (\tilde{\mathbf{x}}_j \cdot \mathcal{L}_j \tilde{\mathbf{c}})^2 \leq 0,$$

which ensures that \tilde{V} is nonincreasing.

Theorem 8. *Let $\mathbf{f}_k(t) = \mathbf{f}(\mathbf{r}_k, t)$ be a three-dimensional, time-varying flowfield that satisfies assumptions A1–A3 in Section 3.1.2. Assume the particle communication topology is defined by an undirected, connected, and time-invariant graph G , with graph Laplacian L . All solutions of the closed-loop model (3.18), where the speed $s_k(t)$ is given by (3.8) and the control $\tilde{\nu}_k$ by (4.17) converge to the set $\{\dot{\tilde{V}} = 0\}$, where \tilde{V} is defined in (4.16). The set of circular formations with radius $|\omega_0|^{-1}$ and direction of rotation determined by ω_0 , is uniformly asymptotically stable and all other positive limit sets are unstable.*

Proof. The closed-loop dynamics (3.18) with $\tilde{\nu}_k$ given in (4.17) depend on the time-varying speed $s_k(t)$. Therefore, the proof follows from application of an invariance-

like theorem for non-autonomous systems [15, Theorem 8.4], stated in Theorem 3 in Chapter 2. The potential \tilde{V} is radially unbounded and positive-definite in the reduced space of relative centers. The time derivative of \tilde{V} satisfies $\dot{\tilde{V}} \leq 0$ and neither \tilde{V} nor $\dot{\tilde{V}}$ depend explicitly on time. The potential \tilde{V} is zero if and only if $\tilde{\mathbf{c}}_k = \tilde{\mathbf{c}}_j \forall j, k \in \mathcal{N}$. By 3 all solutions converge to the set $\{\dot{\tilde{V}} = 0\}$, in which $\tilde{\mathbf{x}}_k \cdot \mathcal{L}_k \tilde{\mathbf{c}} = 0 \forall k$. When $\mathcal{L}_k \tilde{\mathbf{c}} = 0 \forall k \in \mathcal{N}$, the potential \tilde{V} is minimized, forming the set of circular formations $\tilde{\mathbf{c}}_k = \tilde{\mathbf{c}}_j \forall k, j \in \mathcal{N}$. Since this set corresponds to the global minimum of \tilde{V} , it is asymptotically stable, uniformly in time. This set contains circular trajectories on the same of opposite sides of the sphere. Suppose M particles are on one side of the sphere and $N - M$ particles are on the other side. By considering the change in \tilde{V} as a function of a variation of a particle in either group, we observe that (i) if N is even, then solutions with $M = N/2$ are local maxima; and (ii) for any $N > 2$, solutions with $N > M > 0$ are saddles. Therefore, all solutions consisting of colocated circular trajectories on opposite sides of the sphere are unstable. \square

Note, Theorem 8 guarantees positive invariance of the set of circular formations when $\mathbf{f}_k(t) = \mathbf{f}_k(0)$. Figure 4.7(a) illustrates the stabilization of a circular formation in a time-varying flow generated by two point vortices. The vortex strength is given by Γ . The flow due to M point vortices on the surface of a sphere is [21]

$$\mathbf{f}_i = \frac{1}{4\pi\rho_0} \sum_{j=1; j \neq i}^M \Gamma_j \frac{\mathbf{r}_j \times \mathbf{r}_i}{\rho_0^2 - \mathbf{r}_i \cdot \mathbf{r}_j}, \quad (4.18)$$

where ρ_0 is the radius of the sphere and \mathbf{r}_j is the position of a vortex relative to the center of the sphere. A sample integration of (4.18) with $M = 2$ is shown in

Appendix D. We make the assumptions that the vortices effect the motion of the particles, but the particles do not effect the motion of the vortices. In Figure 4.7(a) we show that the particles in model (3.18) are stabilized into a circular formation near the vortices using control (4.17).

4.3.3 Circular Formation with a Prescribed Center

With control (4.17) the center of the circular formation depends on the initial conditions of the particles. We introduce a virtual particle (indexed at $k = 0$) with dynamics given by (3.18) with $\nu_0 = \omega_0 s_0(t)$, so that $\tilde{\mathbf{c}}_0(t) = \tilde{\mathbf{c}}_0(0) \forall t$.

Let $G = (\mathcal{N}, E)$, where $\mathcal{N} = \{1, \dots, N\}$, denote a time-invariant, undirected, and connected graph with edge set E and graph Laplacian L [7]. Also, let $G_0 = (\mathcal{N}_0, E_0)$, where $\mathcal{N}_0 = \{0, 1, \dots, N\}$, denote a time-invariant and directed graph rooted to node 0. The edge set $E_0 \subset E$ includes at least one link from particle 0 to a particle $k \in \mathcal{N}$. L_0 is the Laplacian matrix of G_0 . Consider the augmented potential

$$\tilde{V}_0 = \frac{1}{2} \sum_{(j,k) \in E_0} \|\tilde{\mathbf{c}}_k - \tilde{\mathbf{c}}_j\|^2 = \frac{1}{2} \tilde{\mathbf{c}}^T \mathcal{L} \tilde{\mathbf{c}} + \frac{1}{2} \sum_{j=1}^N a_{j0} \|\tilde{\mathbf{c}}_j - \tilde{\mathbf{c}}_0\|^2,$$

where $a_{j0} = 1$ if there is information flow from particle 0 to particle $j \in \mathcal{N}$, and $a_{j0} = 0$ otherwise. The time-derivative of \tilde{V}_0 along solutions of (3.18) is

$$\begin{aligned} \dot{\tilde{V}}_0 &= \sum_{j=1}^N \dot{\tilde{\mathbf{c}}}_j \cdot \mathcal{L}_j \tilde{\mathbf{c}} + \sum_{j=1}^N a_{j0} \dot{\tilde{\mathbf{c}}}_j \cdot (\tilde{\mathbf{c}}_j - \tilde{\mathbf{c}}_0) \\ &= \sum_{j=1}^N (s_j(t) - \omega_0^{-1} \nu_j) [\tilde{\mathbf{x}}_j \cdot (\mathcal{L}_j \tilde{\mathbf{c}} + a_{j0} (\tilde{\mathbf{c}}_j - \tilde{\mathbf{c}}_0))]. \end{aligned}$$

Choosing

$$\tilde{\nu}_k = \omega_0 (s_k(t) + K_0 \tilde{\mathbf{x}}_k \cdot [\mathcal{L}_k \tilde{\mathbf{c}} + a_{k0} (\tilde{\mathbf{c}}_k - \tilde{\mathbf{c}}_0)]), \quad (4.19)$$

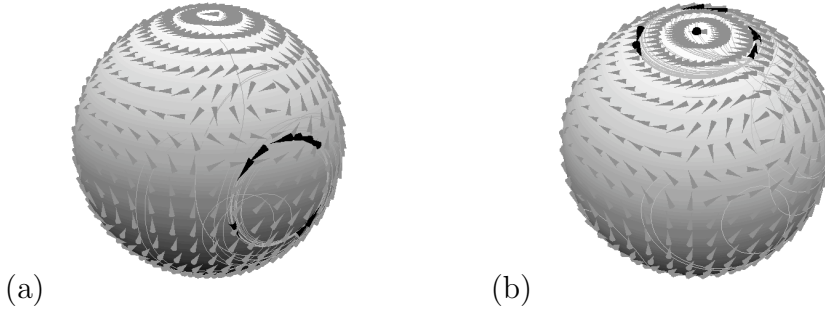


Figure 4.7: Stabilization of a circular formation using model (3.18) in a time-varying flowfield generated by two point vortices. Parameter values are $N = 10$, $\rho_0 = 3$, $\omega_0 = 2$, $K_0 = 0.1$, and $\omega_1 = 0.05$. The strength of the vortices are $\Gamma_1 = 2$ and $\Gamma_2 = 1$. (a) Using control (4.17) the center of the formation is arbitrary. (b) Using control (4.19) the center of the formation is prescribed, in this case at the north pole of the sphere.

makes

$$\dot{\tilde{V}}_0 = -K_0 \sum_{j=1}^N [\tilde{\mathbf{x}}_j \cdot (\mathcal{L}_j \tilde{\mathbf{c}} + a_{j0} (\tilde{\mathbf{c}}_j - \tilde{\mathbf{c}}_0))]^2 \leq 0,$$

which ensures that \tilde{V}_0 is non-increasing.

Corollary 4. *Let $\mathbf{f}_k(t) = \mathbf{f}(\mathbf{r}_k, t)$ be a three-dimensional, time-varying flowfield that satisfies assumptions A1–A3 in Section 3.1.2. Assume the particle communication topology is defined by a time-invariant, undirected, and connected graph G , with graph Laplacian L . Let $G_0 \subset G$ be a time-invariant and directed graph rooted to node 0, with graph Laplacian L_0 . All solutions of the closed-loop model (3.18), where the speed $s_k(t)$ is given by (3.8) and the control v_k by (4.19), converge to the set $\{\dot{\tilde{V}}_0 = 0\}$, where \tilde{V}_0 is defined in (4.19). The set of circular formations is asymptotically stable and all other positive limit sets are unstable. This set corresponds to colocated circular trajectories on the same or opposite sides of the sphere with center $\tilde{\mathbf{c}}_0$, chordal radius $|\omega_0|^{-1}$ and direction of rotation determined by the sign of ω_0 . All*

solutions consisting of colocated circular trajectories on opposite sides of the sphere are unstable.

Corollary 4 provides a method of stabilizing circular formations in a time-varying flowfield on a rotating sphere in model (3.18) with a prescribed center. To simulate our results we use two point vortices generating the time-varying flowfield. In Figure 4.7(b) we use control (4.19) to stabilize a formation of $N = 10$ particles to a center located at the north pole of the sphere.

Chapter 5

Conclusion

In this thesis we present a framework to design decentralized control algorithms for a system of particles in a time-varying flowfield in three dimensions and on the surface of a rotating sphere. Specifically, we provide control laws to stabilize parallel formations with arbitrary and prescribed direction in three dimensions. We also provide control laws to stabilize helical formations in three dimensions with arbitrary pitch and center and prescribed pitch and center. Helical formations are of particular interest because they can be used to stabilize a system of unmanned vehicles that travel in a hurricane or tornado to better predict the intensity of the phenomenon. In the spherical model, we provide control laws to stabilize circular formations on a rotating sphere with arbitrary and prescribed center. The spherical model is of interest because the rotating sphere depicts the Earth spinning on its axis, and we model vortices on the sphere to depict ocean currents or hurricanes.

In real-world applications it is desirable to regulate particle spacing within the formations. This has been achieved in flow-free models in the plane [34] and on a sphere [24]. In ongoing work we wish to regulate particle spacing for both the three-dimensional and spherical model in a time-varying flowfield.

One of the challenges of using the decentralized control laws designed in this thesis for real-world applications is the need to consider strong, varying flows in our

models. We have assumed that the flow does not exceed the speed of the particle relative to the flow. In ongoing work we wish to design control laws in models where the flow exceeds the particle's velocity relative to the flow as well as to simulate the control laws in real flow data.

Appendix A

Transformation Between Relative and Inertial Path Frames

We consider separately the following three individual cases: (i) $t_k(t) \neq 0$ and $v_k(t) \neq 0$; (ii) $t_k(t) = 0$ and $v_k(t) \neq 0$ (or $v_k(t) = 0$ and $t_k(t) \neq 0$); and (iii) $t_k(t) = v_k(t) = 0$. For each case, we provide the transformation between the \mathcal{C}_k and \mathcal{D}_k frames and an analytical expression for each component of \mathbf{u}_k in terms of the components of $\tilde{\mathbf{u}}_k$ and $\mathbf{f}_k(t)$ for model (3.3).

Let θ be the angle between \mathbf{x}_k and $\tilde{\mathbf{x}}_k$, such that $0 \leq \theta \leq \pi$, which implies

$$\begin{aligned}\cos \theta &= \mathbf{x}_k \cdot \tilde{\mathbf{x}}_k = \frac{1 + p_k(t)}{s_k(t)} \\ \sin \theta &= \|\mathbf{x}_k \times \tilde{\mathbf{x}}_k\| = \frac{\sqrt{t_k^2(t) + v_k^2(t)}}{s_k(t)}.\end{aligned}\tag{A-1}$$

Case i If $t_k(t) \neq 0$ and $v_k(t) \neq 0$, we define the unit vector $\mathbf{d} = [d_1 \ d_2 \ d_3]^T$ to be orthogonal to the plane spanned by \mathbf{x}_k and \mathbf{f}_k , i.e.,

$$\mathbf{d} = \frac{\mathbf{x}_k \times \mathbf{f}_k}{\|\mathbf{x}_k \times \mathbf{f}_k\|} = \frac{-v_k(t)\mathbf{y}_k + t_k(t)\mathbf{z}_k}{\sqrt{t_k^2(t) + v_k^2(t)}}.$$

The rotation matrix ${}^{\mathcal{D}_k}R^{\mathcal{C}_k}$ that relates frames \mathcal{C}_k and \mathcal{D}_k is [20]

$${}^{\mathcal{D}_k}R^{\mathcal{C}_k} = \begin{bmatrix} \cos \theta & d_3 \sin \theta & -d_2 \sin \theta \\ -d_3 \sin \theta & d_2^2 \mu_\theta + \cos \theta & -d_2 d_3 \mu_\theta \\ d_2 \sin \theta & -d_2 d_3 \mu_\theta & d_3^2 \mu_\theta + \cos \theta \end{bmatrix},\tag{A-2}$$

where $d_2 = -v_k(t)/\sqrt{t_k^2(t) + v_k^2(t)}$, $d_3 = t_k(t)/\sqrt{t_k^2(t) + v_k^2(t)}$, ($d_1 = 0$), $\cos \theta$ and $\sin \theta$ are given by (A-1), and $\mu_\theta = 1 - \cos \theta$.

Using (A-2), we relate the unit vectors in D_k and C_k by

$$\begin{bmatrix} \tilde{\mathbf{x}}_k \\ \tilde{\mathbf{y}}_k \\ \tilde{\mathbf{z}}_k \end{bmatrix} = {}^{\mathcal{D}_k}R^{\mathcal{C}_k} \begin{bmatrix} \mathbf{x}_k \\ \mathbf{y}_k \\ \mathbf{z}_k \end{bmatrix}. \quad (\text{A-3})$$

If $t_k(t) \neq 0$ and $v_k(t) \neq 0$, we first compute the time derivative of (3.7) and use (3.1) to obtain

$$\begin{aligned} \frac{d}{dt} \tilde{\mathbf{x}}_k &= \left[\frac{d}{dt} \left(\frac{1+p_k(t)}{s_k(t)} \right) - \frac{t_k(t) + v_k(t)}{s_k(t)} \right] \mathbf{x}_k \\ &+ \left[\frac{(1+p_k(t))q_k - v_k(t)w_k}{s_k(t)} + \frac{d}{dt} \left(\frac{t_k(t)}{s_k(t)} \right) \right] \mathbf{y}_k \\ &+ \left[\frac{d}{dt} \left(\frac{v_k(t)}{s_k(t)} \right) + \frac{(1+p_k(t))h_k + t_k(t)w_k}{s_k(t)} \right] \mathbf{z}_k. \end{aligned} \quad (\text{A-4})$$

We then use (A-3) to compare the components of (A-4) to the components of $\dot{\tilde{\mathbf{x}}}_k$ given in (3.3). The expressions for h_k , q_k , and w_k are

$$h_k = \tilde{h}_k + \frac{\dot{p}_k(t) + t_k(t)(\tilde{q}_k - q_k)}{v_k(t)} - \frac{\dot{s}_k(t)(1+p_k(t))}{s_k(t)v_k(t)} \quad (\text{A-5})$$

$$\begin{aligned} q_k &= \frac{\dot{s}_k(t)t_k(t)}{s_k(t)(1+p_k(t))} + \frac{w_kv_k(t) - \dot{t}_k(t)}{1+p_k(t)} + \frac{\tilde{q}_kt_k^2(t)}{t_k^2(t) + v_k^2(t)} \\ &+ \frac{\tilde{q}_ks_k(t)v_k^2(t) - h_kv_k(t)t_k(t)[s_k(t) - (1+p_k(t))]}{(1+p_k(t))[t_k^2(t) + v_k^2(t)]} \end{aligned} \quad (\text{A-6})$$

$$\begin{aligned} w_k &= \frac{\dot{s}_k(t)v_k(t)}{s_k(t)t_k(t)} + \frac{v_k(t)(1+p_k(t))}{t_k(t)} \frac{\tilde{h}_kv_k(t) + \tilde{q}_kt_k(t)}{t_k^2(t) + v_k^2(t)} \\ &- \frac{h_k(1+p_k(t)) - \dot{v}_k(t)}{t_k(t)} + \frac{s_k(t)}{t_k(t)} \frac{\tilde{h}_kt_k(t) - \tilde{q}_kv_k(t)}{t_k^2(t) + v_k^2(t)} \end{aligned} \quad (\text{A-7})$$

Since in this case we assumed that neither $t_k(t)$ nor $v_k(t)$ are equal to zero, $s_k(t) > 0$, and $p_k(t) \neq -1$, (A-5)–(A-7) are nonsingular. Also, the derivatives exist because $\mathbf{f}_k(t)$ is differentiable in t .

Case ii If $t_k(t) = 0$ and $v_k(t) \neq 0$, using (A-2) and (A-3), the relationship between \mathcal{C}_k and \mathcal{D}_k reduces to

$$\begin{bmatrix} \tilde{\mathbf{x}}_k \\ \tilde{\mathbf{z}}_k \end{bmatrix} = \begin{bmatrix} \cos \theta & \sin \theta \\ -\sin \theta & \cos \theta \end{bmatrix} \begin{bmatrix} \mathbf{x}_k \\ \mathbf{z}_k \end{bmatrix}, \quad (\text{A-8})$$

and \mathbf{y}_k and $\tilde{\mathbf{y}}_k$ are equal. If $t_k(t) = 0$ and $v_k(t) \neq 0$, we use (A-8) to compare the components of (A-4) to the components of $\dot{\tilde{\mathbf{x}}}_k$ in (3.3). The expressions for h_k , q_k , and w_k are

$$h_k = \tilde{h}_k + \frac{s_k(t)}{v_k(t)} \frac{d}{dt} \left(\frac{1 + p_k(t)}{s_k(t)} \right) \quad (\text{A-9})$$

$$q_k = \frac{s_k(t)\tilde{q}_k + v_k(t)w_k}{1 + p_k(t)} \quad (\text{A-10})$$

$$w_k = \frac{h_k + \tilde{h}_k}{s_k(t)} \quad (\text{A-11})$$

Equations (A-9)–(A-11) are nonsingular since $v_k(t) \neq 0$, $p_k(t) \neq -1$, and $s_k(t) > 0$ by assumption. The case when $v_k(t) = 0$ and $t_k(t) \neq 0$ follows similarly.

Case iii If $t_k(t) = v_k(t) = 0$, then frames \mathcal{C}_k and \mathcal{D}_k are equal, since \mathbf{x}_k and $\tilde{\mathbf{x}}_k$ are parallel. (\mathbf{x}_k and $\tilde{\mathbf{x}}_k$ cannot be anti-parallel since we have assumed particle k always makes forward progress relative to the flow.) In this case, $\mathbf{u}_k = \tilde{\mathbf{u}}_k$.

Appendix B

Proof of Theorem 4

Let \mathbf{b} be a unit vector orthogonal to $\tilde{\mathbf{x}}_k$ in the plane spanned by \mathbf{x}_k and $\mathbf{f}_k(t)$ as shown in Figure 3.1(b). Let ϕ denote the angle between $\tilde{\mathbf{x}}_k$ and $\mathbf{f}_k(t)$, such that $0 \leq \phi \leq \pi$. We have

$$\begin{aligned}\cos \phi &= \frac{\mathbf{f}_k(t) \cdot \tilde{\mathbf{x}}_k}{\|\mathbf{f}_k(t)\|} \\ \sin \phi &= \frac{\mathbf{f}_k(t) \cdot \mathbf{b}}{\|\mathbf{f}_k(t)\|}.\end{aligned}$$

It is also true that

$$\frac{\|\tilde{\mathbf{x}}_k \times \mathbf{f}_k(t)\|}{\|\mathbf{f}_k(t)\|} = |\sin \phi|,$$

which implies

$$\|\tilde{\mathbf{x}}_k \times \mathbf{f}_k(t)\| = |\mathbf{f}_k(t) \cdot \mathbf{b}|.$$

Also, the fact that $\mathbf{x}_k = (\mathbf{x}_k \cdot \tilde{\mathbf{x}}_k)\tilde{\mathbf{x}}_k + (\mathbf{x}_k \cdot \mathbf{b})\mathbf{b}$ implies

$$\|\mathbf{x}_k\|^2 = (\mathbf{x}_k \cdot \tilde{\mathbf{x}}_k)^2 + (\mathbf{x}_k \cdot \mathbf{b})^2 = 1.$$

Taking the dot product of $\tilde{\mathbf{x}}_k$ and both sides of the speed equation $s_k(t)\tilde{\mathbf{x}}_k = \mathbf{x}_k + \mathbf{f}_k(t)$, and then doing the same with \mathbf{b} , yields

$$\begin{aligned}s_k(t) &= \mathbf{x}_k \cdot \tilde{\mathbf{x}}_k + \mathbf{f}_k(t) \cdot \tilde{\mathbf{x}}_k \\ 0 &= \mathbf{x}_k \cdot \mathbf{b} + \mathbf{f}_k(t) \cdot \mathbf{b}.\end{aligned}$$

We have

$$\begin{aligned}
s_k(t) &= \pm\sqrt{1 - (\mathbf{x}_k \cdot \mathbf{b})^2} + \mathbf{f}_k(t) \cdot \tilde{\mathbf{x}}_k \\
&= \pm\sqrt{1 - (\mathbf{f}_k(t) \cdot \mathbf{b})^2} + \mathbf{f}_k(t) \cdot \tilde{\mathbf{x}}_k \\
&= \pm\sqrt{1 - \|\tilde{\mathbf{x}}_k \times \mathbf{f}_k(t)\|^2} + \mathbf{f}_k(t) \cdot \tilde{\mathbf{x}}_k.
\end{aligned} \tag{B-1}$$

Of the two solutions for $s_k(t)$ provided by (B-1) only the positive root yields $s_k(t) > 0$. The fact that the negative root leads to a negative solution for $s_k(t)$ can be proven by contradiction. Assume that $s_k(t) = -\sqrt{1 - \|\tilde{\mathbf{x}}_k \times \mathbf{f}_k(t)\|^2} + \mathbf{f}_k(t) \cdot \tilde{\mathbf{x}}_k > 0$.

Observe that

$$\|\tilde{\mathbf{x}}_k \times \mathbf{f}_k(t)\|^2 + (\tilde{\mathbf{x}}_k \cdot \mathbf{f}_k(t))^2 = \|\mathbf{f}_k(t)\|^2 < 1.$$

Then we have

$$\begin{aligned}
s_k(t) &< -\sqrt{1 - (1 - (\mathbf{f}_k(t) \cdot \tilde{\mathbf{x}}_k)^2)} + \mathbf{f}_k(t) \cdot \tilde{\mathbf{x}}_k \\
&= -|\mathbf{f}_k(t) \cdot \tilde{\mathbf{x}}_k| + \mathbf{f}_k(t) \cdot \tilde{\mathbf{x}}_k \leq 0,
\end{aligned}$$

which is a contradiction with the assumption that $s_k(t) > 0$. Therefore, the inertial speed of particle k in flow \mathbf{f} is

$$s_k(t) = \sqrt{1 - \|\tilde{\mathbf{x}}_k \times \mathbf{f}_k(t)\|^2} + \mathbf{f}_k(t) \cdot \tilde{\mathbf{x}}_k.$$

Appendix C

Derivation of the Coriolis Acceleration

In Section 3.2.2, we derive the particle dynamics on a rotating sphere assuming the Coriolis acceleration is $-2\boldsymbol{\omega}_1 \times \dot{\mathbf{r}}_k$. Here, we derive the particle dynamics by only knowing the angular velocity vector of the sphere, $\boldsymbol{\omega}_1$.

Taking the cross-product of the angular velocity ${}^{\mathcal{I}}\boldsymbol{\omega}^{\mathcal{C}_k}$ with a unit vector in frame \mathcal{C}_k yields the inertial time-derivative of the unit vector, e.g., $\frac{{}^{\mathcal{I}}d}{dt}\mathbf{x}_k = {}^{\mathcal{I}}\boldsymbol{\omega}^{\mathcal{C}_k} \times \mathbf{x}_k$.

We have

$$\frac{{}^{\mathcal{I}}d}{dt}\mathbf{x}_k = (\cos \phi_k(\dot{\theta}_k + \omega_1) + \dot{\gamma}_k)\mathbf{y}_k - (\sin \phi_k \sin \gamma_k(\dot{\theta}_k + \omega_1) + \cos \gamma_k \dot{\phi}_k)\mathbf{z}_k \quad (\text{C-1})$$

$$\frac{{}^{\mathcal{I}}d}{dt}\mathbf{y}_k = -(\cos \phi_k(\dot{\theta}_k + \omega_1) + \dot{\gamma}_k)\mathbf{x}_k - (\sin \phi_k \cos \gamma_k(\dot{\theta}_k + \omega_1) - \sin \gamma_k \dot{\phi}_k)\mathbf{z}_k \quad (\text{C-2})$$

$$\begin{aligned} \frac{{}^{\mathcal{I}}d}{dt}\mathbf{z}_k &= (\sin \phi_k \sin \gamma_k(\dot{\theta}_k + \omega_1) + \cos \gamma_k \dot{\phi}_k)\mathbf{x}_k \\ &+ (\sin \phi_k \cos \gamma_k(\dot{\theta}_k + \omega_1) - \sin \gamma_k \dot{\phi}_k)\mathbf{y}_k. \end{aligned} \quad (\text{C-3})$$

The inertial kinematics of particle k expressed as vector components in frame \mathcal{C}_k are computed as follows. The position of particle k with respect to O is $\mathbf{r}_k = \rho_0 \mathbf{z}_k$.

The velocity is

$$\begin{aligned} \frac{{}^{\mathcal{I}}d}{dt}\mathbf{r}_k &= \left[(\sin \phi_k \sin \gamma_k(\dot{\theta}_k + \omega_1) + \cos \gamma_k \dot{\phi}_k)\mathbf{x}_k \right. \\ &\quad \left. + (\sin \phi_k \cos \gamma_k(\dot{\theta}_k + \omega_1) - \sin \gamma_k \dot{\phi}_k)\mathbf{y}_k \right]. \end{aligned} \quad (\text{C-4})$$

The acceleration $\frac{{}^{\mathcal{I}}d^2}{dt^2}\mathbf{r}_k$ is found similarly.

The force that acts on particle k on the non-rotating sphere is $\mathbf{F}_k = -N_k \mathbf{z}_k + u_k \mathbf{y}_k$, (given in (3.10)). Also, using Newton's second law, $\mathbf{F}_k = m_k \frac{\mathcal{I}d^2}{dt^2} \mathbf{r}_k$, and $\frac{\mathcal{I}d^2}{dt^2} \mathbf{r}_k$, we obtain

$$\begin{aligned} 0 &= 2 \cos \phi_k \sin \gamma_k (\dot{\theta}_k + \omega_1) \dot{\phi}_k + \sin \phi_k \sin \gamma_k \ddot{\theta}_k \\ &\quad + \cos \gamma_k \ddot{\phi}_k - \sin \phi_k \cos \phi_k \cos \gamma_k (\dot{\theta}_k + \omega_1)^2 \end{aligned} \quad (\text{C-5})$$

$$\begin{aligned} u_k s_0 &= 2 \cos \phi_k \cos \gamma_k (\dot{\theta}_k + \omega_1) \dot{\phi}_k + \sin \phi_k \cos \gamma_k \ddot{\theta}_k \\ &\quad - \sin \gamma_k \ddot{\phi}_k + \sin \phi_k \cos \phi_k \sin \gamma_k (\dot{\theta}_k + \omega_1)^2 \end{aligned} \quad (\text{C-6})$$

$$N_k = \sin^2 \phi_k (\dot{\theta}_k + \omega_1)^2 + \dot{\phi}_k^2. \quad (\text{C-7})$$

We solve (C-5) and (C-6) to obtain the equations of motion for θ_k and ϕ_k ,

$$\begin{aligned} \ddot{\theta}_k &= \frac{1}{\sin \phi_k} (u_k s_0 \cos \gamma_k - 2 \cos \phi_k (\dot{\theta}_k + \omega_1) \dot{\phi}_k) \\ \ddot{\phi}_k &= -u_k s_0 \sin \gamma_k + \sin \phi_k \cos \phi_k (\dot{\theta}_k + \omega_1)^2. \end{aligned} \quad (\text{C-8})$$

We now derive the dynamics of particle k in the sphere-fixed frame, \mathcal{I}' . We have the kinematic relationship

$$\dot{\mathbf{r}}_k \triangleq \frac{\mathcal{I}'d}{dt} \mathbf{r}_k = \frac{\mathcal{I}d}{dt} \mathbf{r}_k \Big|_{\omega_1=0}$$

By assumption, the movement of particle k relative to the sphere-fixed frame is parallel to \mathbf{x}_k , which implies $\dot{\mathbf{r}}_k \cdot \mathbf{y}_k = 0$. We also know that the particle speed relative to \mathcal{I}' is $\rho_0 s_0$, i.e., $\|\dot{\mathbf{r}}_k\| = \rho_0 s_0$. Applying these two constraints to $\dot{\mathbf{r}}_k$ using (C-4) with $\omega_1 = 0$ yields

$$\begin{aligned} \sin \phi_k \cos \gamma_k \dot{\theta}_k - \sin \gamma_k \dot{\phi}_k &= 0 \\ \sin \phi_k \sin \gamma_k \dot{\theta}_k + \cos \gamma_k \dot{\phi}_k &= s_0. \end{aligned} \quad (\text{C-9})$$

We solve (C-9) to obtain

$$\sin \gamma_k = \frac{\sin \phi_k \dot{\theta}_k}{s_0} \text{ and } \cos \gamma_k = \frac{\dot{\phi}_k}{s_0}. \quad (\text{C-10})$$

We use the same procedure to find the dynamics of \mathcal{C}_k in frame \mathcal{I}' . Applying (C-9) to (C-1)–(C-3) yields

$$\begin{aligned} \dot{\mathbf{x}}_k &\triangleq \frac{\mathcal{I}'d}{dt} \mathbf{r}_k = \frac{\mathcal{I}'d}{dt} \mathbf{r}_k \Big|_{\omega_1=0} = \nu_k \mathbf{y}_k - s_0 \mathbf{z}_k \\ \dot{\mathbf{y}}_k &= \frac{\mathcal{I}'d}{dt} \mathbf{r}_k = \frac{\mathcal{I}'d}{dt} \mathbf{r}_k \Big|_{\omega_1=0} = -\nu_k \mathbf{x}_k \\ \dot{\mathbf{z}}_k &= \frac{\mathcal{I}'d}{dt} \mathbf{r}_k = \frac{\mathcal{I}'d}{dt} \mathbf{r}_k \Big|_{\omega_1=0} = s_0 \mathbf{x}_k, \end{aligned} \quad (\text{C-11})$$

where

$$\nu_k = \cos \phi_k \dot{\theta}_k + \dot{\gamma}_k.$$

Differentiating $\sin \gamma_k$ given in (C-10) with respect to time and using (C-8), we find

$$\nu_k = u_k - 2\omega_1 \cos \phi_k = u_k - 2\omega_1 z_{k3},$$

which is the same as (3.13).

Appendix D

The 2-Vortex Problem

Using (4.18), the flow due to $M = 2$ point vortices on the surface of a sphere reduces to [21]

$$\begin{aligned}\mathbf{f}_1 &= \frac{1}{4\pi\rho_0}\Gamma_2\frac{\mathbf{r}_2 \times \mathbf{r}_1}{\rho_0^2 - \mathbf{r}_1 \cdot \mathbf{r}_2} \\ \mathbf{f}_2 &= \frac{1}{4\pi\rho_0}\Gamma_1\frac{\mathbf{r}_1 \times \mathbf{r}_2}{\rho_0^2 - \mathbf{r}_2 \cdot \mathbf{r}_1}.\end{aligned}$$

$3M$ equations are needed to solve the M -vortex problem on a sphere [21]. However, the constraint that the vortices lie on the surface of the sphere reduces the system to $2M$ equations. The Hamiltonian of the system (4.18) for $M = 2$ is [21]

$$H = \frac{\Gamma_1\Gamma_2}{4\pi\rho_0} \log(l_{12}^2) = \text{constant}, \quad (\text{D-1})$$

where l_{12} is the chordal distance between the two vortices. From H we can conclude that the distance between two vortices remains fixed, so that all solutions form relative equilibria. Also, the center of vorticity,

$$\mathbf{C} = \frac{\Gamma_1\mathbf{r}_1 + \Gamma_2\mathbf{r}_2}{\Gamma_1 + \Gamma_2} = \text{constant}, \quad (\text{D-2})$$

is an invariant of the system.

Equations (D-1) and (D-2) give rise to the four equations necessary to solve the problem. In general, two vortices will each move on the base of a fixed cone whose plane is perpendicular to \mathbf{C} . The vortex with a larger Γ will move on the

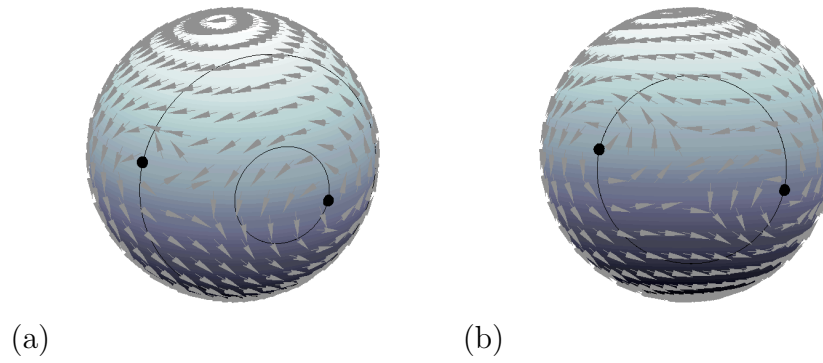


Figure D.1: Two point vortices generate a time-varying flow as they travel on the surface of a sphere. (a) The vortex with strength $\Gamma_1 = 0.5$ moves on the smaller base of the cone and the vortex with strength $\Gamma_2 = 0.2$ moves on the larger one. (b) The vortices with $\Gamma_1 = \Gamma_2 = 0.5$ move around the same circle, opposite of each other.

base of the cone of smaller radius (see Figure D.1(a)). If $\Gamma_1 = \Gamma_2$, the vortices will move on the same plane perpendicular to \mathbf{C} on opposite sides of the same cone (see Figure D.1(b)).

Appendix E

Proof of equation (4.3)

In Sections 4.1 and 4.2 we use the fact that

$$\mathbf{b} \cdot [(\mathbf{a} \times \mathbf{b}) \times \mathbf{a}] = \|\mathbf{a} \times \mathbf{b}\|^2, \quad (\text{E-1})$$

where $\mathbf{a} = [a_1 \ a_2 \ a_3]^T$ and $\mathbf{b} = [b_1 \ b_2 \ b_3]^T$, to show that the time derivative of the Lyapunov functions we use are negative semi-definite. The proof of (E-1) follows.

Let $\mathbf{c} = [c_1 \ c_2 \ c_3]^T$ be the cross product of $\mathbf{a} \times \mathbf{b}$,

$$\mathbf{c} = \mathbf{a} \times \mathbf{b} = \begin{vmatrix} \hat{\mathbf{i}} & \hat{\mathbf{j}} & \hat{\mathbf{k}} \\ a_1 & a_2 & a_3 \\ b_1 & b_2 & b_3 \end{vmatrix} = \begin{vmatrix} a_2 & a_3 \\ b_2 & b_3 \end{vmatrix} \hat{\mathbf{i}} - \begin{vmatrix} a_1 & a_3 \\ b_1 & b_3 \end{vmatrix} \hat{\mathbf{j}} + \begin{vmatrix} a_1 & a_2 \\ b_1 & b_2 \end{vmatrix} \hat{\mathbf{k}}. \quad (\text{E-2})$$

The left hand side of (E-1) can be expanded by using the determinant

$$\mathbf{b} \cdot [(\mathbf{a} \times \mathbf{b}) \times \mathbf{a}] = \mathbf{b} \cdot [\mathbf{c} \times \mathbf{a}] = \begin{vmatrix} b_1 & b_2 & b_3 \\ c_1 & c_2 & c_3 \\ a_1 & a_2 & a_3 \end{vmatrix}. \quad (\text{E-3})$$

When switching rows of a determinant, the determinant changes sign. From (E-3)

we have

$$\begin{aligned}
 \mathbf{b} \cdot [(\mathbf{a} \times \mathbf{b}) \times \mathbf{a}] &= - \begin{vmatrix} c_1 & c_2 & c_3 \\ b_1 & b_2 & b_3 \\ a_1 & a_2 & a_3 \end{vmatrix} = \begin{vmatrix} c_1 & c_2 & c_3 \\ a_1 & a_2 & a_3 \\ b_1 & b_2 & b_3 \end{vmatrix} \\
 &= \begin{vmatrix} a_2 & a_3 \\ b_2 & b_3 \end{vmatrix} c_1 - \begin{vmatrix} a_1 & a_3 \\ b_1 & b_3 \end{vmatrix} c_2 + \begin{vmatrix} a_1 & a_2 \\ b_1 & b_2 \end{vmatrix} c_3 \\
 &= \begin{vmatrix} a_2 & a_3 \\ b_2 & b_3 \end{vmatrix}^2 + \begin{vmatrix} a_1 & a_3 \\ b_1 & b_3 \end{vmatrix}^2 + \begin{vmatrix} a_1 & a_2 \\ b_1 & b_2 \end{vmatrix}^2 = \|\mathbf{a} \times \mathbf{b}\|^2.
 \end{aligned} \tag{E-4}$$

Note that if the vectors \mathbf{a} and \mathbf{b} change positions in the dot and cross products, then

$$\mathbf{a} \cdot [(\mathbf{a} \times \mathbf{b}) \times \mathbf{b}] = -\|\mathbf{a} \times \mathbf{b}\|^2. \tag{E-5}$$

Bibliography

- [1] H. Baruh. *Analytical Dynamics*. Mc Graw-Hill, 1999.
- [2] R. W. Beard, T. W. McLain, D. B. Nelson, D. Kingston, and D. Johanson. Decentralized cooperative aerial surveillance using fixed-wing miniature UAVs. *Proc. IEEE*, 94(7):1306–1324, 2006.
- [3] R. E. Davis, C. E. Eriksen, and C. P. Jones. Autonomous buoyancy-driven underwater gliders. In G. Griffiths, editor, *The Technology and Applications of Autonomous Underwater Vehicles*, chapter 3, pages 37–58. Taylor and Francis, 2002.
- [4] J. A. Fax and R. M. Murray. Graph Laplacians and stabilization of vehicle formations. In *Proc. 15th IFAC World Congress*, pages 283–288, Barcelona, Spain, July 2002.
- [5] R. Fierro, C. Belta, J. P. Desai, and V. Kumar. On controlling aircraft formations. In *Proceedings of IEEE Conference of Decision and Control*, volume 2, pages 1065–1070, Orlando, December 2001.
- [6] P. Fitzpatrick. *Advanced Calculus*. Thomson Corportation, 2nd edition, 2006.
- [7] C. Godsil and G. Royle. *Algebraic Graph Theory*. Number 207 in Graduate Texts in Mathematics. Springer-Verlag, 2001.
- [8] S. Hernandez and D. A. Paley. Stabilization of collective motion in a time-invariant flow field on a rotating sphere. To appear in *Proc. American Control Conf.*, June 2009.
- [9] S. Hernandez and D. A. Paley. Three-dimensional motion coordination in a time-invariant flowfield. To appear in *Proc. Conf. on Decision and Control*, December 2009.
- [10] G. J. Holland, P. J. Webster, J. A. Curry, G. Tyrell, D. Gauntlett, G. Brett, J. Becker, R. Hoag, and W. Vaglianti. The Aerosonde robotic aircraft: A new paradigm for environmental observations. *Bull. American Meteorological Society*, 82(5):889–901, 2001.
- [11] A. Jadbabaie, J. Lin, and A. S. Morse. Coordination of groups of mobile autonomous agents using nearest neighbor rules. *IEEE Trans. Automatic Control*, 48(6):988–1001, 2003.
- [12] E. W. Justh and P. S. Krishnaprasad. A simple control law for UAV formation flying. Technical Report 2002-38, Institute for Systems Research, University of Maryland, 2002.

- [13] E. W. Justh and P. S. Krishnaprasad. Equilibria and steering laws for planar formations. *Systems and Control Letters*, 52(1):25–38, 2004.
- [14] E. W. Justh and P. S. Krishnaprasad. Natural frames and interacting particles in three dimensions. In *Proc. Joint 44th IEEE Conf. Decision and Control and European Control Conf.*, pages 2841–2846, Seville, Spain, December 2005.
- [15] H. K. Khalil. *Nonlinear Systems*. Prentice Hall, third edition, 2002.
- [16] D. B. Kingston. *Decentralized Control of Multiple UAVs for Perimeter and Target Surveillance*. PhD thesis, Department of Electrical and Computer Engineering, Brigham Young University, Provo, Utah, December 2007.
- [17] D. J. Klein and K. A. Morgansen. Controlled collective motion for trajectory tracking. In *Proc. 2006 American Control Conf.*, pages 5269–5275, Minneapolis, Minnesota, June 2006.
- [18] G. Lafferriere, A. Williams, J. S. Caughman, and J. J. P. Veerman. Decentralized control of vehicle formations. *Systems and Control Letters*, 54(9):899–910, 2005.
- [19] N. E. Leonard, D. A. Paley, F. Lekien, R. Sepulchre, D. M. Fratantoni, and R. E. Davis. Collective motion, sensor networks and ocean sampling. *Proc. IEEE*, 95(1):48–74, 2007.
- [20] R. Murray, Z. Li, and S. Sastry. *A Mathematical Introduction to Robotic Manipulation*. CRC Press, 1994.
- [21] P. Newton. *The N-Vortex Problem*. Springer-Verlag, 2001.
- [22] G. Nilsson and R. Vabø. Why do fish swim in circles? how are decisions made when one million fish swim together and act as one until. *Marine Research News*, (1), 2007.
- [23] R. Olfati-Saber and R. M. Murray. Consensus problems in networks of agents with switching topology and time-delays. *IEEE Trans. Automatic Control*, 49(9):1520–1533, 2004.
- [24] D. A. Paley. Stabilization of Collective Motion on a Sphere. *Automatica*, 45(1):212–216, 2009.
- [25] D. A. Paley, N. E. Leonard, and R. Sepulchre. Stabilization of symmetric formations to motion around convex loops. *Systems and Control Letters*, 57(3):209–215, 2008.
- [26] D. A. Paley and C. Peterson. Stabilization of Collective Motion in a Time-Invariant Flowfield. 32(3):771–770, 2009. *AIAA J. Guidance, Control, and Dynamics*.

- [27] Lawrence Perko. *Differential Equations and Dynamical Systems*. Springer, 3rd edition, 2000.
- [28] C. Peterson and D. A. Paley. Cooperative control of unmanned vehicles in a time-varying flowfield. To appear in *Proc. AIAA Guidance, Navigation, and Control Conf.*, invited session on “UAV Complex Atmospheric Conditions”, 2009.
- [29] A. Sarlette, R. Sepulchre, and N. E. Leonard. Cooperative attitude synchronization in satellite swarms: A consensus approach. In *Proc. 17th IFAC Symp. Automatic Control in Aerospace (electronic)*, page 6, Toulouse, France, June 2007.
- [30] L. Scardovi, N. Leonard, and R. Sepulchre. Stabilization of three-dimensional collective motion. *Communication in Information and Systems*, Brockett Legacy issue, accepted. (Preprint: arXiv: 0806.3442).
- [31] L. Scardovi, N. E. Leonard, and R. Sepulchre. Stabilization of collective motion in three dimensions: A consensus approach. In *Proc. 46th IEEE Conf. Decision and Control*, pages 2931–2936, New Orleans, Louisiana, December 2007.
- [32] L. Scardovi, R. Sepulchre, and N. E. Leonard. Stabilization laws for collective motion in three dimensions. To appear in *Proc. European Control Conference*, Kos, Greece, July 2007.
- [33] R. Sepulchre, D. A. Paley, and N. E. Leonard. Stabilization of planar collective motion: All-to-all communication. *IEEE Trans. Automatic Control*, 52(5):811–824, 2007.
- [34] R. Sepulchre, D. A. Paley, and N. E. Leonard. Stabilization of planar collective motion with limited communication. *IEEE Trans. Automatic Control*, 53(3):706–719, 2008.
- [35] T. Vicsek, A. Czirók, E. Ben-Jacob, I. Cohen, O. Shochet, and A. Tenenbaum. Novel type of phase transition in a system of self-driven particles. *Phys. Rev. Lett.*, 75(6):1226–1229, 1995.